Department of Electrical and Computer Engineering

Noise Detection and Elimination in Online Impulse Frequency Response Analysis

Bahar Mohseni

This thesis is presented for the Degree of
Master of Philosophy (Electrical and Computer Engineering) of
Curtin University

March 2017

Declaration

"To the best of my knowledge and belief this thesis contains no material previously published by any other person except where due acknowledgment has been made. This thesis contains no material which has been accepted for the award of any other degree or diploma in any university"

Signature: _____

Bahar Mohseni

Date: 20th April 2017

This thesis is dedicated to the loving memory of my beloved sister Shima Mohseni.

Acknowledgement

I would like to express my most sincere gratitude towards my supervisor, Professor Syed Islam, without whom I would be unable to be in the position to complete this research. Prof Islam's dedication and support towards this research is invaluable and has been my source of motivation throughout the duration of my research. I would also like to express my appreciation towards my associate supervisor, Dr. Naser Hashemnia for his constant help and support throughout this study and all staff and colleagues at the Department of ECE of Curtin University, especially Mark Fowler.

I would like to thank my parents, who have never stopped believing in me, and their continuous love and support and my older brother Mansour who has never ceased to kindly hold my hand and show me the way.

Last but not least, my God.

Abstract

Online impulse frequency response analysis (IFRA) offers substantial benefits for continuous assessment of the transformer condition to avoid unexpected failure and ensure power delivery. However, applying the online IFRA technique involves some problems associated with the transformer being connected to the power grid as the test is being conducted. One of the problems is that measured signals acquired at substation environments are coupled with extensive noise, which exhibit different distribution properties.

The presence of the noise can lead to different responses with no actual change in the transformer winding and thereby, misinterpretation of the results. Therefore, signal de-noising is an essential process for accurately extracting the response signals from the acquired noise-corrupted signals before further analysis. To this end, initially, the distribution properties of different types of noise and their impact on the transformer frequency response analysis (FRA) have to be investigated and secondly, based on the derived results, appropriate approaches need to be taken to eliminate the noise. Also, improvements need to be made on the mathematical procedure applied to signals in the time domain to determine their frequency content to help obtain a more reliable frequency response from the measured data.

Publications

[1] Bahar Mohseni, Naser Hashemnia, Ahmed Abusiada, Syed Islam, "On the Development of Online Frequency Response Analysis of Transformers–Denoising Signal Interferences," in preparation for submission to Industrial Electronics, IEEE Transactions, 2017.

[2] Bahar Mohseni, Naser Hashemnia, Syed Islam, " Online Detection of Partial Discharge inside Power Transformer Winding Through IFRA," accepted for presentation in Power and Energy Society General Meeting (PES), 2017 IEEE, 2017.

[3] Bahar Mohseni, Naser Hashemnia, , Syed Islam, " Application of S Transform for Detection of External Interferences in Online Transformer Impulse
Frequency Response Analysis," accepted for presentation in IEEE International Conference on Environment and Electrical Engineering, 2017 IEEE, 2017.

[4] Bahar Mohseni, Naser Hashemnia, Zhongyong Zhao, Syed Islam, " Application of Online Impulse Technique to Diagnose Inter-turn Short Circuit in Transformer Windings," Australasian Universities Power Engineering Conference (AUPEC), 2016.

[5] Bahar Mohseni, Naser Hashemnia, Syed Islam, "Condition Assessment of Power Transformer Bushing Using SFRA and DGA as Auxiliary Tools," International Conference on Power Systems Technology (POWERCON), 2016.

[6] Naser Hashemnia, , A. Aziz Ashrafian, Bahar Mohseni, Syed Islam, " Improved Power Transformer Bushing Fault Detection Based on Signal Processing," TECHON conference, Bristol United Kingdom, 2016.

Contents

DECLARATION II

ACKNOWLEDGEMENT IV

ABSTRACT V

PUBLICATIONS VI

CONTENTS VII

LIST OF FIGURES IX

LIST OF TABLES XI

ACRONYMS XII

1. INTRODUCTION 1

1.1 INTRODUCTION 1

1.2 THE OBJECTIVES OF THESIS 3

1.3 THE OUTLINE OF THESIS 4

2. BACKGROUND 5

2.1 INTRODUCTION 5

2.2 WINDING DEFORMATION 5

2.2.1 Axial Forces 6

2.2.2 Radial Forces 8

2.2.3 Other Forces 9

2.3 WINDING DEFORMATION DETECTION 9

2.3.1 Offline Detection Methods 9

2.3.2 Online Detection Methods 10

2.4 FREQUENCY RESPONSE ANALYSIS 11

2.5 FRA STANDARDS 14

2.5.1 IEC 60076-18 15

2.5.2 IEEE C57.149 15

2.6 FRA ON WINDING DEFORMATION 16

2.7 ANALYZATION AND INTERPRETATION OF FRA MEASUREMENT 17

2.8 SIGNAL PROCESSING 17
2.8.1 Fast Fourier Transform 18
2.8.2 Continuous Wavelet Transform 19
2.9 FILTERING AND DE-NOISING 20
2.10 NOISE REMOVAL USING DWT 20
2.11 SUMMARY 21

3. SIMULATION METHOD 30

3.1 INTRODUCTION 30
3.2 TRANSFORMER FINITE ELEMENT MODELLING 31
3.2.1 Parameter calculation 32
3.2.2 Inductance and resistance matrices calculation 33
3.2.3 Capacitance matrix calculation 34
3.3 POST PROCESSING 35
3.4 TRANSFORMER MODELLING CASE STUDIES 36
3.5 MECHANICAL FAULT SIMULATION 42
3.6 SIMULATION OF NOISE AND EXTERNAL INTERFERENCES 44
3.6.1 External pulse-shaped interferences 45
3.6.2 Internal pulsive discharge between winding sections 46
3.6.3 Background noise 48

4. SIGNAL PROCESSING 49

4.1 INTRODUCTION 49
4.2 GENERALIZED S TRANSFORM *50*
4.3 HYPERBOLIC S TRANSFORM *51*
4.4 APPLICATION OF HST IN THE DETECTION OF ABNORMANILITIES *52*
4.4.1 Case study 1 52
4.4.2 Case study 2 57

5. FILTERING TECHNIQUE 61

5.1 INTRODUCTION *61*
5.2 FILTER DESIGN *62*

5.3 OBTAINING THE FILTERED RESPONSE *64*

5.4 VERIFICATION OF THE PROPOSED FILTERING TECHNIQUE *65*

6. EXPERIMENTAL WORK ON ONLINE IFRA METHOD 68

6.1 INTRODUCTION *68*

6.2 TEST SYSTEM CONFIGURATION 69

6.2.1 Nanosecond pulse generator 69

6.2.2 Signal injection and protection circuit 70

6.2.3 Capacitive coupling circuit and capacitive voltage divider 72

6.3 EXPERIMENTAL RESULTS *73*

6.3.1 Offline impulse frequency response test 73

6.3.2 Online impulse frequency response test 75

6.4 Application of the proposed filtering technique to test results 76

7. CONCLUSIONS AND FURTHER RESEARCH 78

8. REFERENCE 80

List of Figures

Figure 2-1 World energy consumption by region (in quadrillion Btu)

Figure 2.1. HV and LV wind Flux lines and forces Directions

Figure 2.2: Axial displacement

Figure 2.3: Axial bending

Figure 2.4: Conductor tilting

Figure 2.5: Two types of buckling a) forced buckling, b) free buckling Figure

2.6: Inter-turn fault.

Figure 2.7. Central frequency and Fourier transform of Morlet wavelet

Figure 2.8. Central frequency and Fourier transform of mofified-Morlet wavelet

Figure 2.9. Decomposition tree used for MRA analysis

Figure 2.10. Decomposition tree of de-noising using DWT

Figure 3.1. Inductance/capacitance matrix configurations for a three-disk winding

Figure 3.2. Transformer geometrical design details

Figure 3.3. Transformer 3D finite element model

Figure 3.4. Maxwell SPICE circuit

Figure 3.5. 3D model of Bushing solved in electrostatic FEM solver

Figure 3. 6. Simulation signals a) input voltage, b) output current

Figure 1.7. Power Transformer 3D model

Figure 3. 8. Simulation signals a) input voltage, b) output current

Figure 3.9. 3` model of the deformed winding

Figure3.10. Free buckling deformation

Figure 3.11. Input voltage a) pure sine wave b) switching transient

Figure 3.12. Output current variation internal partial discharge vs normal condition

Figure 3.13. Background noise added to output current

Figure 4.1. Variation of hyperbolic window with different frequencies

Figure 4.2. 3D finite element model of the deformed winding

Figure 4.3.The impact of internal mechanical fault on a) transformer online IFRA signature b) timefrequency contour of the output current.

Figure 4.4. The impact of external pulsive noise on healthy winding a) transformer online IFRA signature b) time-frequency contour of the output current in the event of external pulse with IFRA impulse

Figure 4.5. The impact of external pulsive noise on winding with internal mechanical fault on transformer online IFRA signature and time-frequency contour of the output current

Figure 4.6.The impact of background noise on transformer online IFRA signature andtime-frequency contour of the output current.

Figure 4.7. Variation of IFRA signature as a result of internal pulsive discharge between winding sections

Figure 4.8. Free buckling deformation on online IFRA signature and time--frequency contour of the output current
Figure 5.1. Need for linear time variant filters []

Figure 5.2. Intensity image derived from transformer output current time-frequency contour

Figure 5.3. Time frequency filter mask to filter time-limited band-limited noise with variation threshold value

Figure5.4. Faulty winding in the presence of background and pulsive noise online IFRA signature and time-frequency contour of the output current in the noisy condition

Figure 5.5. Time-frequency contour of the output current after filtering implementation and filtered transformer online IFRA signature Figure 6.1. Test schematic configuration

Figure 6.2. Nanosecond impulse generator

Figure 6.3. Capacitive coupling mounted on bushing

Figure 6.4. Signal injection and protection circuit

Figure 6.5. Signal injection and output measurement

Figure 6.6. Online test setup

Figure 6.7. Transformer under test

Figure 6.8. Measurement results a) input voltage b) output current c) transformer offline IFRA signature

Figure 6.9. Measurement results a) input voltage b) output current c) transformer offline IFRA signature

Figure 6.10. Transformer offline (red) and online (blue) IFRA signatures a) before and b) after applying the filtering technique

List of Tables

Table 2.1: Comparison of main electrical diagnostic techniques for winding deformation

Table 2.2. Number of recommended tests for different transformer types

Table 3.1 Advantages and disadvantages of various modelling techniques

Table 3.2 Bushing Model Parameters

Table 3.3. Dielectric properties of bushing

Acronyms

FRA	Frequency Response Analysis
DSI	Discrete Spectral Interference
DGA	Dissolved Gas Analysis
SCI	Short Circuit Impedance
STFT	Short Time Fourier Transform
MOSFET	Metal–Oxide–Semiconductor Field-Effect Transistor
SNR	Signal to Noise Ratio
CWT	Continuous Wavelet Transform
MRA	Multi-Resolution Analysis
DWT	Discrete Wavelet Transform
HST	Hyperbolic S Transform

1. Introduction

1.1 Introduction

Power transformers are unquestionably one of the most crucial pieces of equipment in electrical power systems. In the sub-transmission and transmission network of a large interconnected power utility, an astounding number of a few hundred to above a thousand transformers from 69 kV to 500 kV can be found excluding the lower voltage distribution network transformers with replacement costs ranging from hundreds to millions of dollars depending on the transformer size. The average life expectancy of power transformers ranges from 25 to 30 years in normal operating conditions, which can be extended to as long as 60 years with proper maintenance. However, as a result of the continuing advancement in electric power transmission and distribution systems and the increasing worldwide transformer population age, the likelihood of transformer catastrophic failures, which in turn leads to power outages, is increasing [1]. Transformer outages are extremely costly and dangerous for power utilities; Hence, the importance of developing a standard diagnosis tool to detect potential mechanical problems, including displacements or deformations [2-4].

Severe abnormal conditions including short circuits, switching transients, lightning strokes and other incidents trigger the deterioration of internal mechanical condition of transformers. With the aging of transformers, their initial electrical and mechanical withstand capability to overcome abnormal conditions decreases. The degradation can burgeon into a point where it can no longer withstand transient over-voltages and short circuit currents. Therefore, it is imperative that utilities maintain the transformers in good operating conditions. Conventionally, routine time-based preventative maintenance combined with regular testing was used. However, the increasing pace of utility expansion and thereby deregulation has resulted in a higher failure risk and hence, the need for developing more sophisticated condition monitoring techniques to prevent catastrophic failures with highs financial costs.

Nowadays, A variety of testing and condition monitoring techniques including

vibration method, current deformation coefficient method, current deformation coefficient method and transfer function method used in utilities for transformer fault detection. The aforementioned techniques will be discussed in more detail in the literature review in chapter 2.

One of the most important problems in transformer diagnostic methods is the diagnosis of winding mechanical movement. As the transformers age, the structure of their insulation compresses, which in turn, leads to the increment of the clamping pressure exerted on the winding which results in winding movement. Also, short circuit forces on the transformer winding are a cause of the transformer mechanical faults, including winding deformations and displacements (axial/radial), winding looseness, clamping pressure defects and core defects. Looseness or distortion of transformer windings can lead to transformer mechanical or electrical failure. Based on the knowledge accumulated from field testing of transformers, the Frequency Response Analysis (FRA) method is perceived as the most effective diagnostic technique for detecting power transformer's mechanical problems including:

- winding deformations and displacements (axial/radial),
- winding looseness,
- clamping pressure defects
- core defects

There is also a growing trend in industry to move from traditional time-based maintenance programs (undertaking maintenance at regular pre-determined time intervals) to condition-based maintenance (carried out when the equipment is suspected to be deteriorating). Hence the need for developing non- intrusive diagnostic methods to assess the internal condition of power transformers while they are in non-stop service working as a part the power system [5]. At least two prerequisites must be fulfilled before the verification of online IFRA as a feasible measurement system:

1) Development of a suitable signal injection system capable of generating controllable repeatable pulses

2) Isolation of the transformer response from external interferences coming from the power system

The first problem has been addressed in studies [6-8] by designing a pulse generator with the capability to produce controlled signals with sufficiently high amplitude and a wide frequency spectrum in the range of MHz.

The focus of this thesis is to overcome the second problem by proposing effective signal processing as well as de-noising techniques to help eliminate the impact of external interferences on the results obtained from online impulse frequency response analysis (IFRA). By using the approach given in this thesis as a block before interpretation of the results and making the final judgement on the transformer mechanical integrity, the chance of misinterpretation of the results due to noise and external interferences is considerably reduced.

1.2 The Objectives of Thesis

This research is aimed at improving online IFRA input and output signals in a way that they uniquely manifest the transformer condition, eliminating the interference of external factors. To this end, the following objectives are to be achieved:

- The first objective of the thesis is to improve the accuracy of the existing transformer high frequency modeling method for online IFRA.

- The second objective of the thesis is to investigate characteristics of various types of noise which may be imposed on the input and output signals during the online IFRA testing.

- The third objective of the thesis is to determine the effect of the noise on the transformer IFRA signature and determine what distinguishes it from the impact of internal mechanical faults

- To design filtering techniques to eliminate the impact of different types of noise from the transformer signature and develop signal de-noising methods for effectively retrieving results not influenced by external interferences

1.3 The Outline of Thesis

This thesis is broken up into several chapters. This first introductory chapter covers the background of transformer condition monitoring techniques specifically Frequency Response Analysis (FRA). The objective and contribution of this thesis is also elaborated in this chapter.

Chapter 2 gives a more detailed narrative on the different types of transformer winding deformations, a classification of transformer winding deformation main diagnostic techniques with utmost/prior attention given to Frequency Response Analysis (FRA), the standards and stages of using this method to detect fault inside the transformer.

In Chapter 3, a simulation method based on finite element modelling (FEM) and circuit analysis is developed for modelling the transformer for online impulse frequency response analysis (IFRA). This modelling technique is used to emulate the behavior of two power transformers under study.

In Chapter 4 the signal processing tool used for mathematical processing of the test signals is described. The impact of external interferences and mechanical deformations on transformer IFRA signature is then studied by taking advantage of this approach.

In chapter 5, a time-frequency filtering technique based on Hyperbolic S Transform (HST) is proposed for online IFRA to eliminate the impact of external interferences and allow for better assessment of the test results.

Chapter 6 presents the experimental setup and presents the measurement results from online IFRA test on a 10 kVA power transformer in a high voltage laboratory. The developed filtering technique is then applied to the measured signals.

2. Background

2.1 Introduction

In order to determine transformer internal status, evaluating the level of of its mechanical integrity is a key factor which must be considered. Slight transformer winding deformations do not necessarily require taking the transformer out of service. However, if left undetected, damage will develop, causing a total failure.

There are two leading causes which lead to internal transformer components mechanical damage. The first factor is associated with electromagnetic forces (EMF) due large rushes of current propagating inside the transformer winding. Fast generation of large EMFs can result in instability of the transformer winding structure. Shock-loading during the installation and commissioning process or transportation of a transformer is one of the other factors affecting this issue [9]. Several cases of transformer internal mechanical damage] as a result of improper handling during transportation were presented in CIGRE 2009 6th Southern Africa Regional Conference [7]. Possible damages include bending of clamping rod, displacement of core and broken clamping structure. In such situations, any damage to the transformer winding physical structure can result in costly affairs and delays in power network operation.

An international survey of large power transformers condition monitoring implemented by CIGRE [10] demonstrates that the rate of failure in transformers ranges from 1% to 2% per year. While the survey shows a fairly low failure rate amongst transformers, one single incipient fault in large power transformers usually acquires large financial costs. Therefore, transformer condition monitoring is one of the key priorities for utilities to prevent the faults from burgeoning into catastrophic failures and forced outages.

2.2 Winding Deformations

In the presence of magnetic fields, conductors carrying currents, magnetic forces will be exerted on the conductor. As indicated in Equation 2.1, the flux density and current density are proportional to the forces under which the winding of the transformer is working. Therefore, a direct relation exists between the square root of the current passing through the winding and the forces it experiences.

This leads to doubling the forces on the transformer winding as a result of the occurrence of short-circuit with respect to the normal operation condition which exceeds the transformer rated current [13].

$$F = \mathrm{L}\,(I \times B) \tag{2.1}$$

In (2.1), L is the transformer winding length, I shows the current passing through the winding and B represents the magnetic field. The direction of forces is vertical to the flux direction. In addition, the components which make up the leakage flux including the radial Bx and the axial denoted By. Therefore, the radial component of the flux Bx forms the axial component of the forces Fy and By crafts the radial component of forces i.e. Fx. The radial forces as presented in Figure 2.1 manifest the constant inward forcing of the internal and the external winding undergoes outward forces, which result in forced buckling and free buckling (hoop buckling), respectively.

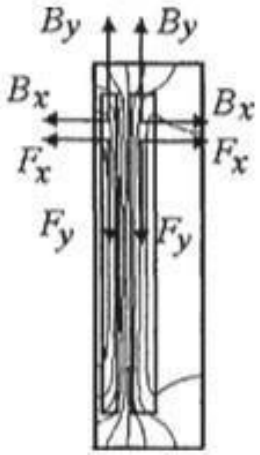

Figure 2.1. Directions of forces and HV and LV Flux lines [11]

2.2.1 Axial Forces

Failure modes which happen as a result of axial forces on the winding structure include bending, tilting of conductors and axial displacement. It is crucial for transformer HV winding and LV winding to be perfectly in line with respect to each other and the center line. The movement of each transformer windings can lead to uneven distribution of forces, which will, in turn, lead to the increase of axial forces in both windings [12]. In the case of excess of axial forces, transformer windings will be vertically displaced from their

aligned original position, leading to the damage of the winding clamping structure

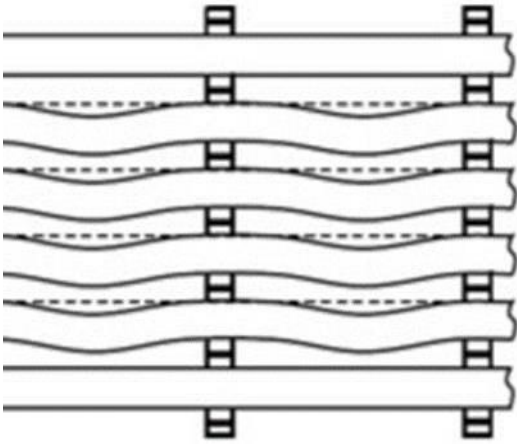

Figure 2.3: Axial bending

As shown in Figure 2.4, if the axial force exerted on the winding exceeds the allowable axial compressive force limit on the winding structure, winding conductors respond to the force with tilting. According to [9], conductor tilting

can result in the damage of insulation.

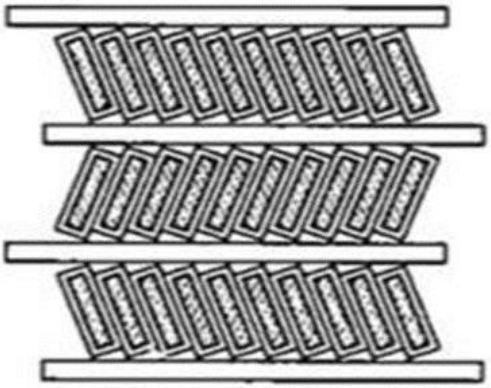

Figure 2.4: Conductor tilting

2.2.2 Radial Forces

The internal winding is continuously subject to radial forces which act as compressive stress in inward direction whereas the outer winding expriences radial forces in an outward direction causing tensile stress. There is a higher chance of winding being damaged by tensile stress than compressive stress [11].

Compressive stress on the inner winding, however, can lead to buckling as depicted in Figure 2.5, which is a common failure mode on transformer inner winding. When exceeding the conductor materials elastic limit, compressive forces can lead to winding damage referred to as either forced or free-buckling [10], and the buckling shape is ultimately determined by winding support. In the case of winding inner supporting structure, forced buckling would happen.

In the case free-buckling, conductors bend outward as shown in Figure 2.5 (b).

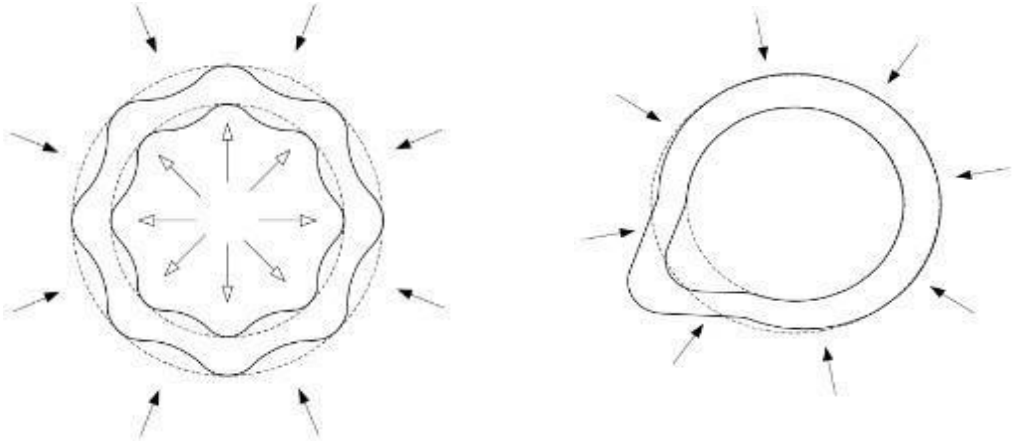

(a) (b)

Figure 2.5: Two types of buckling [11] a) forced buckling, b) free buckling

2.2.3 Other Forces

A number of other mechanical faults occurring at particular points in transformer winding are not in the form of axial or radial forces. A conspicuous instance in this regard is inter-turn short circuit faults which happen due to the degradation of the insulation between two neighboring conductors in the winding of the transformer. As a result of insulation deterioration, hotspots will form in the transformer windings which if not detected in early stages, will result in major failures such as melting of the copper conductors in transformer winding [15].

2.3. Mechanical Deformation Diagnostic Methods

2.3.1 Offline Fault Detection

In the case of external damage to the transformer, inspection can be implemented relatively easily in comparison with to damage being incurred to

Figure 2.6: Inter-turn short circuit fault.

the internal elements. This is primarily due to the fact that the latter requires the power transformer to be taken out of service and electrically disconnected from the power system. Therefore, a number of methodologies have been conducted to diagnose the damage of internal transformer components. A number of the available offline diagnostic methods are shown and compared in Table 2.1. The common drawback of the majority of these techniques is the lack of sufficient sensitivity. Frequency Response Analysis (FRA), however, exhibits a high level of sensitivity as well as good repeatability as a result of various transformer winding mechanical faults.

Table 2.1: Comparison of the available diagnostic tools for transformer winding deformation

Diagnostic Method	Advantages	Disadvantages
Magnetizing current (inrush)	Simple test equipment Capable of detecting core deficiencies.	Insensitive to winding mechanical movements. Measurements significantly influenced by core residual
Impedance (leakage reactance)	Conventional technique Used in short- circuit testing standards Availability of nominal (reference) values.	Small changes of certain kinds can result in significant deviations in the results. For some fault types sensitivity is low (works best for buckling deformations).

Frequency Response of Stray Losses (FRSL)	Has better sensitivity than impedance test Strong detection of short circuit between parallel components.	This standard is not widely used in industry.
Low Voltage Impulse Method (LVI)	Known as a sensitive method	Need for special equipment Prone to unrepeatability features Requires expert interpretation
Frequency Response Analysis	A higher repeatability level w.r.t LVI while having the same sensitivity Interpretation less taxing than the LVI method (results shown in frequency domain instead of time domain).	Needs to be standardized Requires expertise to interpret the test results

2.3.2 Online Fault Detection

Among the existing methods for monitoring the power transformer condition while it is in service working as a part of the power system. Most common online fault detection methods include partial discharge analysis, vibration analysis and dissolved gas analysis. These methods, however, are not adequately capable of detecting transformer winding mechanical deformations.

While online detection of mechanical deformation is not commercially available, it has recently generated significant interest amongst the scientific community. A few online techniques including vibration and ultrasonic techniques, communication method, current, short circuit impedance (SCI), and transfer function measurements [18] have been introduced. Due to the fact that FRA is a becoming growingly popular for the assessment of power transformers' mechanical integrity [19], the main focus of this thesis being on overcoming the challenges associated with the online implementation of FRA, the following sections will be further discussing this method including the implementation technique, different aspect and challenges.

2.4 Frequency Response Analysis

FRA method is a comparison-based method based on the fact that the transformer transfer function (which can be shown as impedance), undergoes variations as a result of transformer winding mechanical deformation. The changes happening in the transformer frequency response referred to as FRA signature allow for both identifying and quantifying the faults.

Different components of transformer structure including HV and LV windings, the core, and the insulation can be shown as equivalent electrical circuits, consisting of self and mutual inductances, resistors, capacitors, and. When a mechanical deformation occurs inside the transformer, the values of these components will be altered which, in turn, leads to the variation of the frequency response signature of the equivalent electrical circuit. The changes of dielectric properties of the insulation materials as a result of moisture ingress, heating or aging of the materials as well as geometrical changes, may affect the transformer FRA signature especially in resonance and anti-resonance [20].

2.5 FRA Standards

2.5.1 IEC 60076-18

Since transformer winding self-inductance value tends to be larger than that of the mutual inductances, the characteristic of the transformer behavior in the low frequency range is mainly influenced by the self-inductance (Lm) of the transformer, as shown in (2.2).

$$L_m = \frac{N^2}{\Re} \tag{2.2}$$

In (2.2) N represents the coil number of turns and $\Re$ denotes the reluctance of the core. By increasing the frequency to the range of mid frequencies, inductive reactance's value will be too high to be taken into account and capacitive reactance starts to play a more pivotal role in forming the transfer function of the transformer. The inductive reactance of mutual inductances, however, will become significant in mid frequencies. In the mid frequency range, which reaches up to a few hundreds of kHz based on the size of the transformer under study and the configuration of its active parts, winding

capacitive components consisting of series (turn to turn and disc to disc capacitances) and ground (the capacitance between and the configuration of its active parts, winding capacitive components consisting of series (turn to turn and disc to disc z) and ground (the capacitance between transformer winding and the core/tank) capacitances and the mutual inductances control the fluctuations of the frequency response. When frequency reaches high values, the leakage and mutual inductances reach values large enough to be overlooked and thereby, the transfer function will go through a rising trend, with the series and ground capacitances becoming more dominant.

As concluded from the aforementioned facts, the variation of transformer FRA signature in low frequencies happen as a result of changes in transformer core. The changes in medium frequency range, however, are controlled by winding characteristics (capacitances as well as mutual inductances) and in high frequency range, ground and series capacitances act as leads.

2.5.2 IEEE C57.149

The IEEE standard on FRA was published in March 2013. However, although the publication was referred to as a standard, it was more of a guide on the application of Frequency Response Analysis on Oil-immersed transformers and the interpretation of the results [26]. Some parts of the standard are, as expected, akin to those of the IEC and CIGRE documents, while some additional details particularly on making the test connections and the failure were also provided by the IEEE standard. With regards to connecting the test components, various testing recommendations exist for different transformer types which can be found in Table 2.2. The evident fact which can be pertained by looking at the table is that the testing prerequisites can differ considerably, with 36 different methods presented. However, given that performing a large number of tests may not be feasible in some cases, the standard, suggests a minimum number of testing required for each type of transformer, which in all cases includes all open circuit and short-circuit tests. The standard also talks about failure modes, including response characteristics based measured outputs from actual case studies. From an FRA user perspective, this is particularly useful in analysing the response from a test as it outlines the important response characteristics [24-25].

Table 2.2. Number of recommended tests for different transformer types [25]

Transformer	Minimum Recommended Test	Total Test Listed
Two winding Transformer	9	15
Autotransformer without tertiary	9	12
Autotransformer with tertiary	18	33
Autotransformer with buried tertiary	9	18
Three winding Transformer Part 1	18	36
Three winding Transformer Part 2	18	36

2.6 FRA on Winding Deformation

A transformer's unique FRA signature is a variable of its inductive and capacitive components. Give the significance of transformer winding as well as its vulnerability to different types of mechanical deformation, most studies in the field of FRA focus on this component of the transformer. In order to fully analyze the impact of winding damage on frequency response of the transformer, different simulation methods have been used as a key tool by many investigators since it is the least cumbersome and expensive method with respect to mechanically deforming real life transformer windings and studying the following impacts. Section 2.7 provides a summary of previous work around the impact of different types of winding deformation and analysis of results. A robust way of analysing the frequency response derived from a transformer and diagnosing the type of transformer winding damage is by knowing the kind of change each type of mechanical deformation brings about in the transformer FRA signature. Simulation studies has so far been the main tool in performing studies on the changes to transformer signature as a result of mechanical damage. It is time and cost efficient and provides researches with the opportunity to perform many case studies and derive accurate results. Although comparing simulation results to measurements from the actual transformer would produce the best results, there are some constraints around building a prototype transformer for this purpose which is capable of reversible mechanical deformations to enable such studies [25]. A useful solution to analyze the response can be developed by understanding the transfer function changes resulting from mechanical deformations.

2.7 Analyzation and Interpretation of FRA Response

FRA is a method used to assess power transformer winding displacement or deformation. In this method, the impedance function of a transformer is obtained in different intervals over time and by comparing this impedance function referred to as "FRA signature" with previous measurements and capturing the differences, the potential type of mechanical damage depending on the frequency band and severity of the deviations can be identified. Therefore, it is necessary to establish a reliable high-frequency model of a power transformer to derive interpretations guidelines for potential failures.

Based on the application, various simulation methods have been used for modelling the transformer winding [25-27]. Over the first 50 years, experimental work was the primary basis. However, as technology evolved, researches and engineers developed techniques to simulate complex phenomena such as injection of high frequency voltage impulses into the transformer windings [28].

In order to derive a more accurate representation of resistive, inductive and capacitive components of the system, it is useful that the magnitude plots are accompanied by phase relationships which together correctly reflect voltage and current waveforms. It is often useful to compare resonance in the magnitude plots with the zero crossings in the phase relationship. Complex wavelet transform and S transform are capable tools for a) capturing the phase angle of each frequency component of the waveform and b) representing time-frequency components of the waveform.

2.8 Signal processing

Signal processing is a process through which waveform measurements are modified and analysed. In the thesis's field of study signal processing is used to derive the frequency content of time domain signals. In the initial studies on FRA, Fast Fourier transform (FFT) was the tool most widely used, one example is studies performed by M.Bagheri et al. [30]. However, due to limitations of this tool, including lack of time vs frequency resolution and only being applicable for periodic signals, its use is debated by M.Bagheri et al. in [31].

Short-time Fourier transform (STFT) improves on FFT by dividing the signal into multiple shorter term windows which allows for determination of an aperiodic signal's

frequency content. However STFT also has resolution issues due to the fixed size of the windowing function.

2.8.1 Fast Fourier Transform (FFT)

Conventionally, FFT is the tool used to convert the signals from time domain to the frequency domain (2.3). However, by definition, this tool is useful for processing stationary signals since it only provides the frequency content of the signal with no information on the time each frequency component has occurred.

$$|TF| = \frac{|FFT(i(t))|}{|FFT(v(t))|} \tag{2.3}$$

2.8.2 Continuous Wavelet Transform (CWT)

Transient signal analysis could be improved by using wavelet transform for signal processing, given its time versus frequency resolution. Wavelet transform is a useful tool for obtaining the frequency-response curve of the transformer in service which has better repeatability compared to FFT and overcomes the nonactual resonant behavior of FFT. Applying cwt on the time domain signals gives us a set of coefficients which are a function of scale and time. Using continuous wavelet transform, the transfer function at any given frequency can be obtained from the energy (rms) value of the output signal divided by that of the input signal. CWT is defined as

$$CWT_{x(t)}(\tau, a) = \frac{1}{\sqrt{a}} \int_{-\infty}^{+\infty} \boldsymbol{x(t)\omega}\left(\frac{\tau - t}{\alpha}\right) \boldsymbol{dt} \tag{2.4}$$

where is the scaling factor, is the time shifting factor, is the mother Wavelet function, and is the signal to be transformed. The energy (rms) value of the measured voltage and current signals at each given scale can be obtained from (2.5)

$$\left\| S_a \right\| = \int_{-\infty}^{+\infty} S_a^2(t)dt = \sqrt{(C_s(\tau, a))^2} \tag{2.5}$$

Where α is the scaling factor, α is the time shifting factor, τ is the mother Wavelet function, and is the signal to be transformed. The energy (RMS) value of the measured voltage and current signals at each given scale can be obtained from IEC 60076-18 [32] .

$$|TF| = \sqrt{\frac{\sum_{\tau}(CWT_{I(t)}(\tau,a))^2}{\sum_{\tau}(CWT_{V(t)}(\tau,a))^2}} \tag{2.5}$$

The Morlet wavelet is normally used as the mother wavelet for obtaining the timefrequency properties of signals. However, the problem with Morlet is that it has a comparatively wide bandwidth which leads to extraction of information from the bandwidth as well as the central frequency. This results in differences between the obtained results and the reference curve. To overcome this problem, a new mother wavelet with a narrower bandwidth taking the Morlet wavelet (2.7) as a reference is added to wavelet toolbox in MATLAB. The new modified wavelet is given in (2.8).

$$\omega(t) = \cos(2\pi t)e^{-0.04t^2} \tag{2.7}$$

$$\omega(t) = \cos(2\pi t)e^{-0.04t^2} \tag{2.8}$$

2.9 Filtering and de-noising

To date, there has been little headway in the area of filtering electrical signals coming from the power system in online IFRA. In [33] a mathematical filtering technique based on the coherence function is presented and [24] merely mentions the need for eliminating the aliasing effect.

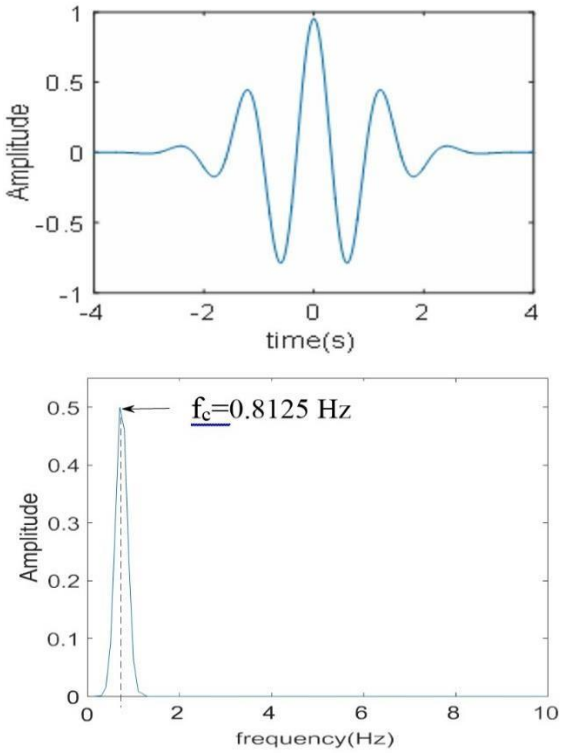

Figure 2.7. Central frequency and Fourier transform of Morlet wavelet

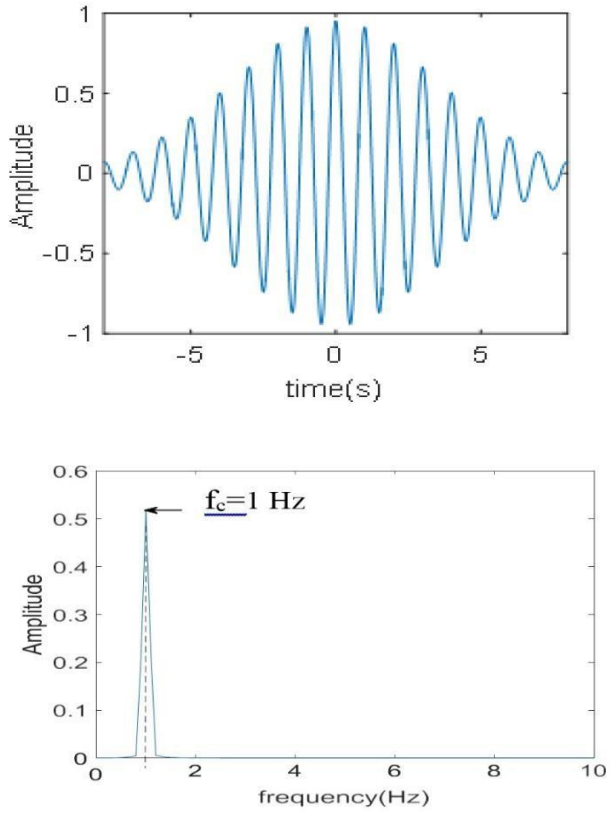

Figure 2.8. Central frequency and Fourier transform of mofified-Morlet wavelet

2.10 Noise Removal using DWT

Conventionally, analogue filters (e.g., high pass filter (HPF) and low pass filter (LPF)) or Fourier transform are used to remove the noise. However, these methods require a prior knowledge on particular frequencies of the noise, which are normally unknown in practice. Recently, wavelet transform (WT) has attracted attention on signal denoising. It does not require the knowledge on frequencies of noise and can analyze the time-frequency (TF) characteristic of a signal. Wavelet transform is a signal decomposition technique which consists of trimming the wavelet transform coefficients taking a threshold value as a reference. For filtering and de-noising purposes, the multiresolution analysis within the discrete wavelet transform (DWT) is used. The MRA analysis successively decomposes the signal S(t) into low and high frequency information by means of high- pass and low-pass filters. This decomposition is expressed in terms of two types of coefficients: The approximations which are the low-frequency components of the signal and the details which are the high-frequency components [29].

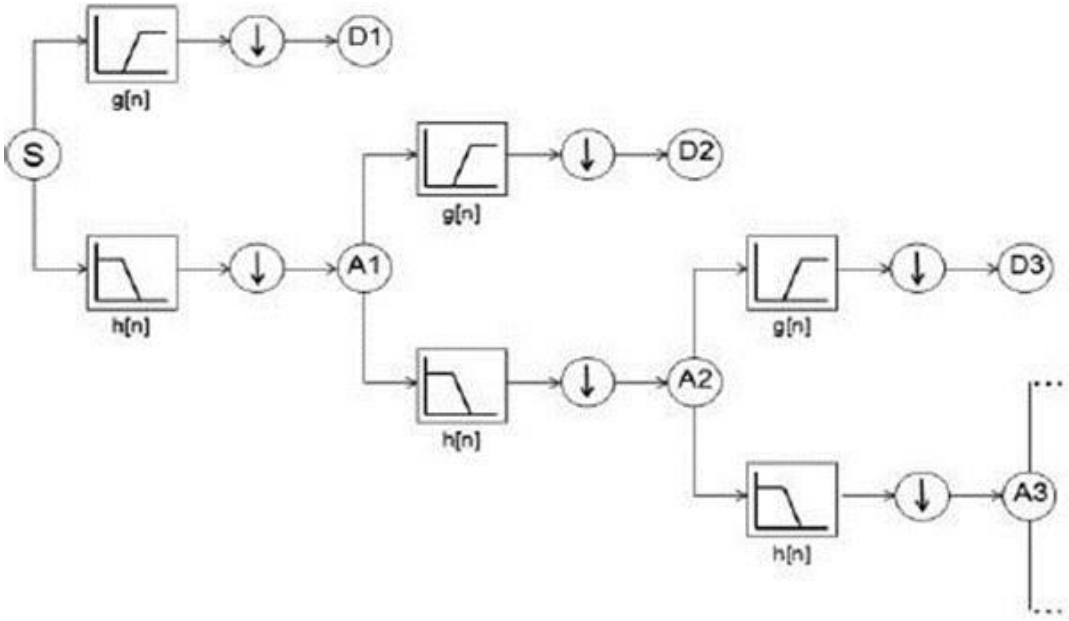

Figure 2.9. Decomposition tree used for MRA analysis

1) Application of DWT for harmonic distortion removal

Based on [35] the best mother wavelet for removing harmonic distortion from power

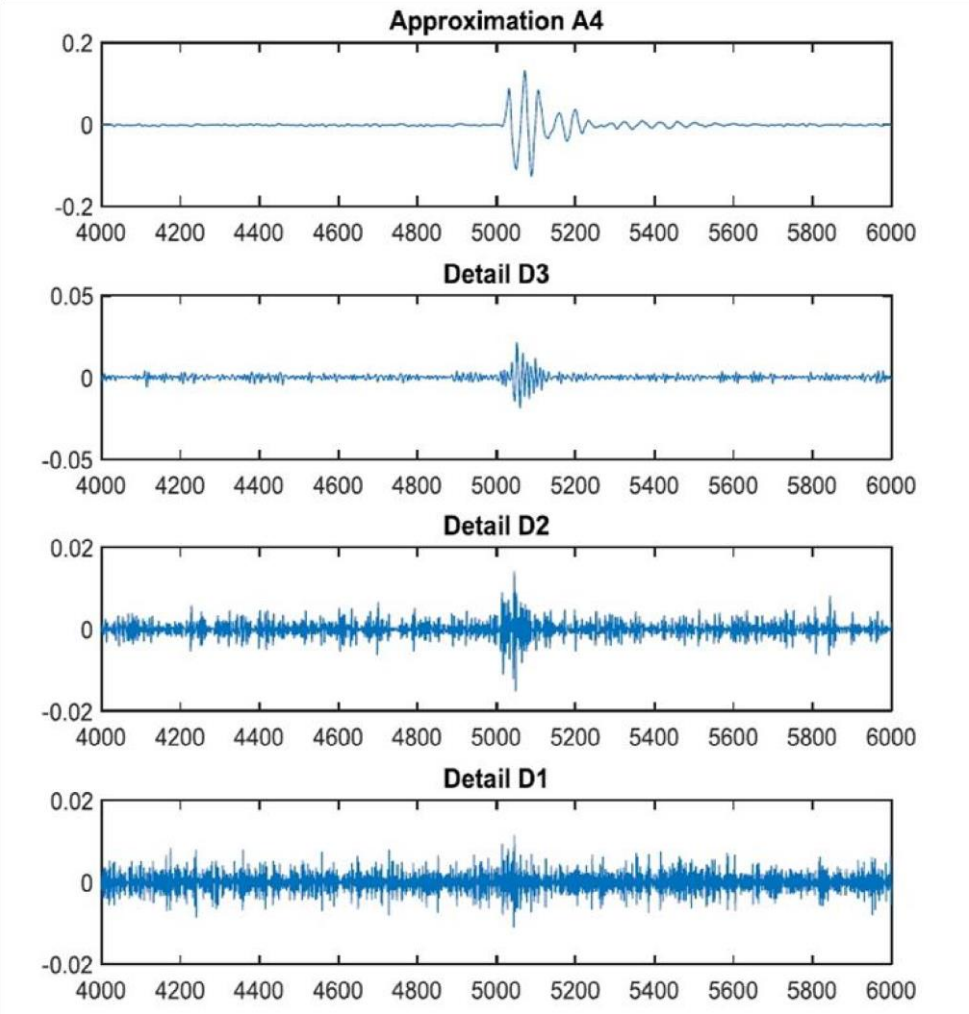

Figure 2.10. Decomposition tree of de-noising using DWT

system signals is Daubechies 7 (db7). Mother wavelet is chosen on the basis of energy criteria, which states the percentage energy deviation at each level from the original signal given by (2.9). The mother wavelet with the minimum overall energy deviation for all decomposition levels is chosen as the most suitable.

$$\%\delta E(n) = \frac{E_a - E_{an}}{E_n} \tag{2.9}$$

Where $\%\delta E_n$ denotes percentage energy deviation at nth decomposition level from signal's overall energy E_a and E_{an} is energy content of the signal at nth level of decomposition. The selection of decomposition level is another important aspect of DWT. The signal is decomposed up to the level till fundamental component is separated from the harmonic components depending on the signal under study.

2) Application of DWT for background noise removal

The mother wavelet Daubechies 4 (db4) is commonly used for filtering electrical signals [25]. In [31], a level 4 decomposition with soft thresholding was applied to eliminate the background noise from the measured voltage and current waveforms.

2.11 Summary

The importance of developing diagnostic tests on power transformers in service to enable continuous condition monitoring, prevent unexpected failures and ensure power delivery has been expressed by different authors [8,12]. Among the two existing options to perform the online FRA test (FRA and SFRA), IFRA has reached a better potential for online implementation [3], although the magnitude of the injected pulse can reach more than a thousand volts, the pulse duration is very short. Therefore, the energy of the pulse is small and it would not have a considerable impact on the normal operation of the transformer in service. While the majority of the available literature have opted for online IFRA [3,7], some researches have availed online SFRA [15] stating the random occurrence of the uncontrolled transient signals (such as switching pulses and lightning strokes) and complication of signal processing in online IFRA as their reasons for choosing SFRA over IFRA. The former problem is observed in [8, 9] which use high-voltage transients inherent to the normal operation of the electrical network as the input for online IFRA. This is troublesome since the measured frequency response curve depends on the shape of transients which may vary from one measurement to another. However, recent attempts have been made to address this issue by designing online signal injection and measurement systems. Tom De Rybel et al [7] developed an online monitoring system injecting high frequency signals on a 650 kV transformer through bushing tap. In [31] an electronic circuit is used to inject microsecond pulses with adjustable properties (amplitude, width and phase) through a capacitor.

Reference [12] proposed a pulse signal generator which injects controllable nanosecond pulses with high amplitudes to the terminals of transformer winding through a capacitive coupling sensor which is metal strap wrapped around the bushing. The response is measured using a Rogowski coil that can handle wide bandwidth signals Once the injection and measurement of the input and output signals are covered, filtering and mathematical processing of the signal come up.

Reference [13] points out the need to filter the aliasing effect of electrical signals coming from the power grid and in [14] a mathematical filtering technique based on the coherence function is proposed.

Gomez et al [15] have suggested multiresolution analysis within the discrete wavelet transform (DWT) for filtering out the power system harmonics and eliminating background noise [16] coupled with the measured signals. This method works with filter banks applied to discrete signals, which constitutes natural filtering. After de-noising, mathematical processing applied to the signals to determine their frequency content and construct the FRA curve.

The common tool used by the majority of operators for the mathematical procedure is the fast Fourier transformation (FFT). However, FFT is not the best choice as it is useful in processing stationary signals. In [32] the use of continuous wavelet transform (CWT) is proposed to overcome the non-repetitive effects and nonactual resonant behavior of the FFT. In [18] the application of S-transform as superior mathematical tool for FRA applications is proposed.

3. Simulation Method

3.1 Introduction

Transformer modelling play a substantial role to determine the characteristics of transformer dynamic behavior and to simulate the transient response of the transformer due to different excitations, the internal resonance and finally calculating the transfer function of the transformer.

To date, an extensive amount of work has been done on transformer modelling, with the studies coming to the fruition of analytical models to emulate the transient behavior of transformer winding. Although these models suffer from limitations in terms of accuracy and miss details of a real transformer geometry, they are considered as a convenient method for analyzing transformer winding mechanical deformations since it is generally more feasible to conduct a study on winding deformation based on simulation rather than on an actual winding, especially due to the cost factor. In addition, some forms of winding deformation are probably impossible to recreate on an actual winding, such as the tilting of conductors.

The approach to investigating winding deformation using numerical model is recommended by CIGRE in [17]. The document suggests modelling the transformer winding based on the geometrical parameters in order to provide a better understanding and interpretation of FRA responses. It also further mentions that such a method may be able to generate a database of responses from various winding damages. To this end, a number of studies have been conducted to use electromagnetic theory network analysis and geometry as tools for calculating the equivalent circuit parameters of transformer through internal and external models. The methods can be generally categorized as following [3].

1) Internal models

In these models all parts of transformer including winding, core, tank, spacers, etc. are modeled based on the internal physical geometry and properties

2) External models

These models do not require prior knowledge of transformer construction data and are based the input/output characteristics of the transformer measured at the terminals.

The pros and cons of these two type of modeling are tabulated in table 3.1. The suitable model is chosen based on the application for which the modeling is used and the desired frequency spectrum.

Table 3.1 Advantages and disadvantages of various modelling techniques

Type of modelling	Physical models	Black-Box models
Based on	Constructional details	Terminal measurements
Advantages	Enables mechanical deformation simulation	No need for design data Better applicability for online fault detection and interpretation
Disadvantages	requires exclusive manufacturing design records	Performance not guaranteed Not suitable for studying geometrical effects

In this study an approach based on finite element modelling (FEM) and circuit analysis is used for modelling the transformer for online impulse frequency response analysis (IFRA). In this approach, the transformer model is computed using 3D transient solver in the Maxwell package and the resulting sub-circuit is exported into Maxwell SPICE for post-processing. To simulate internal partial discharge inside the transformer winding, a pulse signal is injected between sections of the LV winding in the equivalent Spice circuit. The details of the calculation approach and transformer modeling technique are given in the following sections of this chapter.

3.2 Transformer Finite Element Modelling for Online IFRA

Finite element analysis (FEA) is a sophisticated tool widely used by the scientific and industrial community with the ability to find the solution to any problem which can be described by a set of spatial partial derivative equations with appropriate boundary and initial conditions.

In order to obtain a unique solution to each problem, Maxwell solves the electromagnetic field problems by solving Maxwell's equations in a finite region of space with appropriate boundary conditions and user-specified boundary conditions when necessary. There is in essence three steps to using finite element for solving problems:

1) Meshing the problem space into adjoining elements with suitable geometry and setting proper values for the material properties of each element, including conductivity, permeability and permittivity

2) Setting up the initial condition by exciting the model

3) Specifying the boundary conditions

3.2.1 Parameter Calculation

The 3D (frequency domain or harmonic solver) uses Maxwell formulation for analysis. It is based on the assumption that all electromagnetic fields pulsate at the same frequency (specified by the user) and have magnitudes and initial phase angles calculated by Maxwell. There are no moving objects (velocity is zero everywhere). Permanent magnets cannot be part of the model, and all materials are assumed to be linear. Electromagnetic radiation can also be simulated.

In the non-conducting regions, the magnetic field strength is given by the following equation:

H=H P + Δ ϕ

In regions with non-zero conductivity where eddy current calculation has been set up, the following equation where the electric vector potential is calculated using edge elements is true:

H = H P + ∇ϕ + T

At the interface between conductors and non-conductors, the tangential component of the electric vector potential is constrained to zero. The quantity calculated by Maxwell in this case is the magnetic field H(x,y,z,t). Typical sources for eddy current problems include current and current density. In applying the sources for the magnetic field problems, the applied current distribution must be divergence free in the entire space of the solution as it is physical for (quasi) stationary conduction current density distributions. Thus, the conduction path (s) for the applied current distributions must be closed when totally contained within the solution space for the problem or must begin and end at the boundaries. The total current applied to conductors that touch the boundaries does not require existence of the terminals at the ends where the current is applied; in this case, the respective planar surfaces of the conductors in the plane of the region (background) can be used to apply the excitations.

3.2.2 Inductance and Resistance Matrices Calculation

Maxwell software performs a sequence of magneto-static field simulations in order to compute the inductance matrix of the transformer. A current of one Ampere is allowed to flow in each conductor in each field simulation. For a system comprising of n conductors, n field simulations are performed. As a result the energy of the magnetic field coupling two conductors is

$$W_{ij} = \frac{1}{2}\int_{d\Omega} B_i \times H_i d\Omega \qquad (3.1)$$

In (3.1) Wij represents the energy which links the two conductors, Bi is the magnetic flux density generated by the flow of one ampere current though conductor I and Hj

is the corresponding magnetic field. The inductance which couples the two conductors is then given by

$$L_{ij} = \frac{2W_{ij}}{I^2} = \frac{1}{2}\int_{d\Omega} B_i \times H_i d\Omega \tag{3.2}$$

After the 3D model is solved, the self-inductance and resistance of the ith section can thereby be estimated by using the magnetic energy Wii which is the magnetic energy of the ith section of the winding when it is subject to current I.

For calculating the mutual inductance and resistance between the winding sections I and j can be computed using (3.3) and (3.4).

$$L_{ii} = 2\,\mathrm{Im}(jW_{ii})/I_i^2 \tag{3.3}$$

$$R_{ii} = 2\,\mathrm{Re}(jW_{ii})/I_i^2 \tag{3.4}$$

For calculating the mutual inductance and resistance between the winding sections I and j can be computed using (3.3) and (3.4).

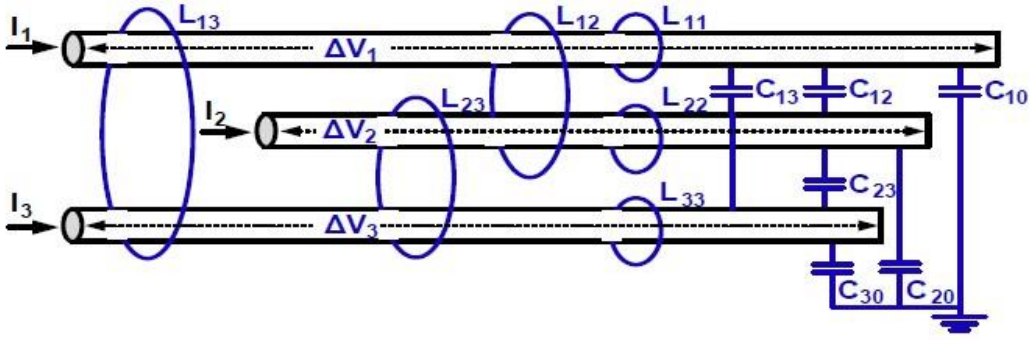

Figure 3.1. Inductance/capacitance matrix configurations for a three-disk winding

$$M_{ij} = \frac{n_i n_j\,\mathrm{Re}\{W_{ij}\} - \frac{1}{2}L_{ii}I_i^2 - \frac{1}{2}L_{jj}I_j^2}{I_i I_j} \tag{3.3}$$

$$R_{ij} = \frac{n_i n_j \omega\,\mathrm{Im}\{W_{ij}\} - \frac{1}{2}R_{ii}I_i^2 - \frac{1}{2}R_{jj}I_j^2}{I_i I_j} \tag{3.4}$$

Wij in the formulae represents the entire magnetic energy when winding sections i and j are excited by currents Ii and Ij .

Based on the current loops of the three-section winding shown in Figure 3.1, the following matrix expresses the relationship between the currents passing through the designated sections and the induced flux in a matrix form

$$\begin{bmatrix} \lambda_1 \\ \lambda_2 \\ \lambda_3 \end{bmatrix} = \begin{bmatrix} L_{11} & L_{12} & L_{13} \\ L_{21} & L_{22} & L_{23} \\ L_{31} & L_{32} & L_{33} \end{bmatrix} \begin{bmatrix} i_1 \\ i_2 \\ i_3 \end{bmatrix} \tag{3.5}$$

3.2.3 Capacitance Matrix Calculation

The electrostatic energy Wel can be used for capacitance matrix calculation in a similar manner to that of the magnetic energy for the calculation of inductance. The electrostatic energy Wel is

$$W_{el} = \frac{1}{2} C V^2 \tag{3.6}$$

The inter-disk and self-capacitance are calculated as follows

$$C_{ij} = \frac{\mathrm{Re}\{W_{el,ij}\} - \frac{1}{2} C_{ii} V_i^2 - \frac{1}{2} C_{jj} V_j^2}{I_i I_j} \tag{3.7}$$

$$C_{ii} = 2 \frac{\mathrm{Re}\{W_{ij}\}}{V_i^2} \tag{3.8}$$

The coupling charge between among a group of conductors is represented by a capacitance. In the case of one unique ground taken as reference for all three conductors shown in Figure 3.1, each object's net charge is given by

$$\begin{bmatrix} Q_1 \\ Q_2 \\ Q_3 \end{bmatrix} = \begin{bmatrix} C_{10} + C_{12} + C_{13} & -C_{12} & -C_{13} \\ -C_{21} & C_{20} + C_{21} + C_{23} & -C_{23} \\ -C_{31} & -C_{32} & C_{30} + C_{31} + C_{32} \end{bmatrix} \begin{bmatrix} V_1 \\ V_2 \\ V_3 \end{bmatrix} \tag{3.9}$$

Any change in winding geometry as a result of mechanical faults will result in the change of capacitance the elements of and inductance matrices of the transformer equivalent circuit.

3.2.4 Post-processing

A review of the available literature on online impulse frequency response analysis (IFRA) shows that after calculating the parameters of transformer using different transformer modelling techniques, they almost unanimously used an equivalent circuit with static parameters to obtain the online transformer response. Although this type of simulation has proven to be useful for offline FRA [36] it fails to emulate the dynamic performance characteristics of in service transformer and its electromagnetic transient behaviour.

In this study a new approach for simulating online transformer IFRA test is proposed. The approach taken in this thesis differs from the previous work in the fact that in this approach, which is based on finite element modelling (FEM) and circuit analysis [37,38] after computing the transformer using 3D transient solver in the Maxwell package, instead of using the values of the calculated parameters to form a linear circuit, the resulting sub-circuit is exported as an equivalent circuit in the format of Maxwell into Maxwell SPICE for postprocessing. In the equivalent Spice Circuit used for studying the terminal behavior of the transformer, the mutual inductance is modelled with a leakage inductance branch for each disk coil which is evaluated at each time step of the simulation process. At each given time step, the leakage and mutual inductances are determined by the level of input current and the back EMF is calculated based on both these variables. To make the modelling more accurate, the additional components including winding resistance, bushing model etc. can be manually added to the Spice model to improve the accordance between the terminal behavior of the experimental case under study and simulation.

This chapter shows how to simulate different abnormalities, the impact of these abnormalities on the results obtained from online transformer IFRA test will be discussed in the following chapter.

A. Case study 1

1) Transformer 3D Finite Element Model

For accurate modeling of transformer using finite element analysis, the design data and structural properties of the transformer under study are required. Figure 3.2 depicts parts of the geometrical details of the transformer under study. The transformer is a three-phase, two-winding, 11-kV/412 V, Dyn1, 50-Hz, 10kVA, oil-immersed, ONAN, core-type distribution transformer. Each winding is comprised of 6 disks, each disk of high voltage winding consisting of 1134 turns and each disk of low voltage winding of 43 turns.

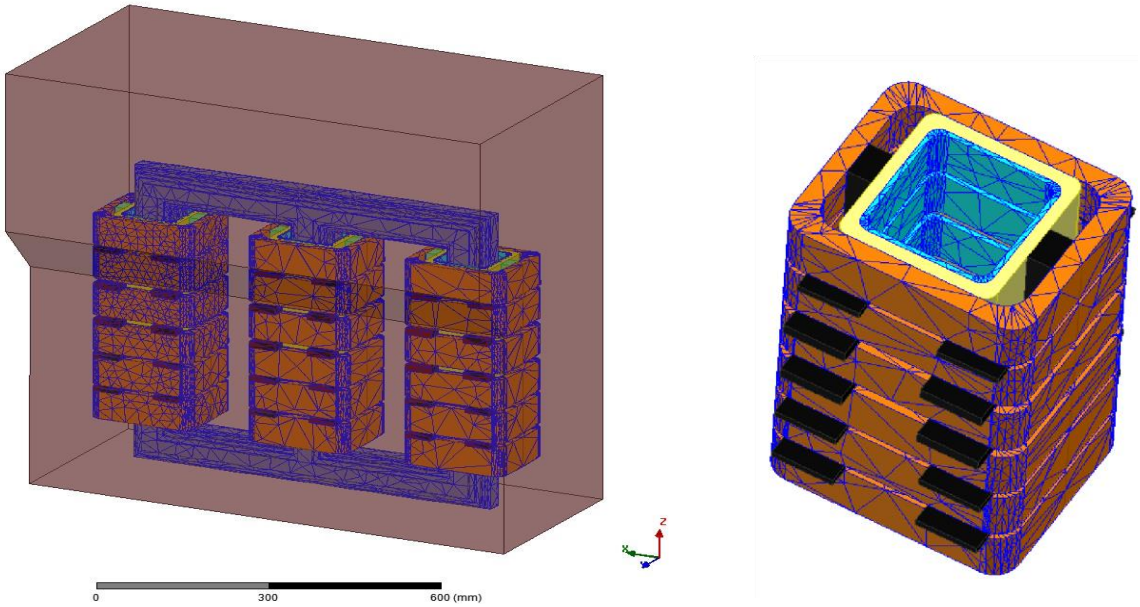

Figure 3.3. Transformer 3D finite element model

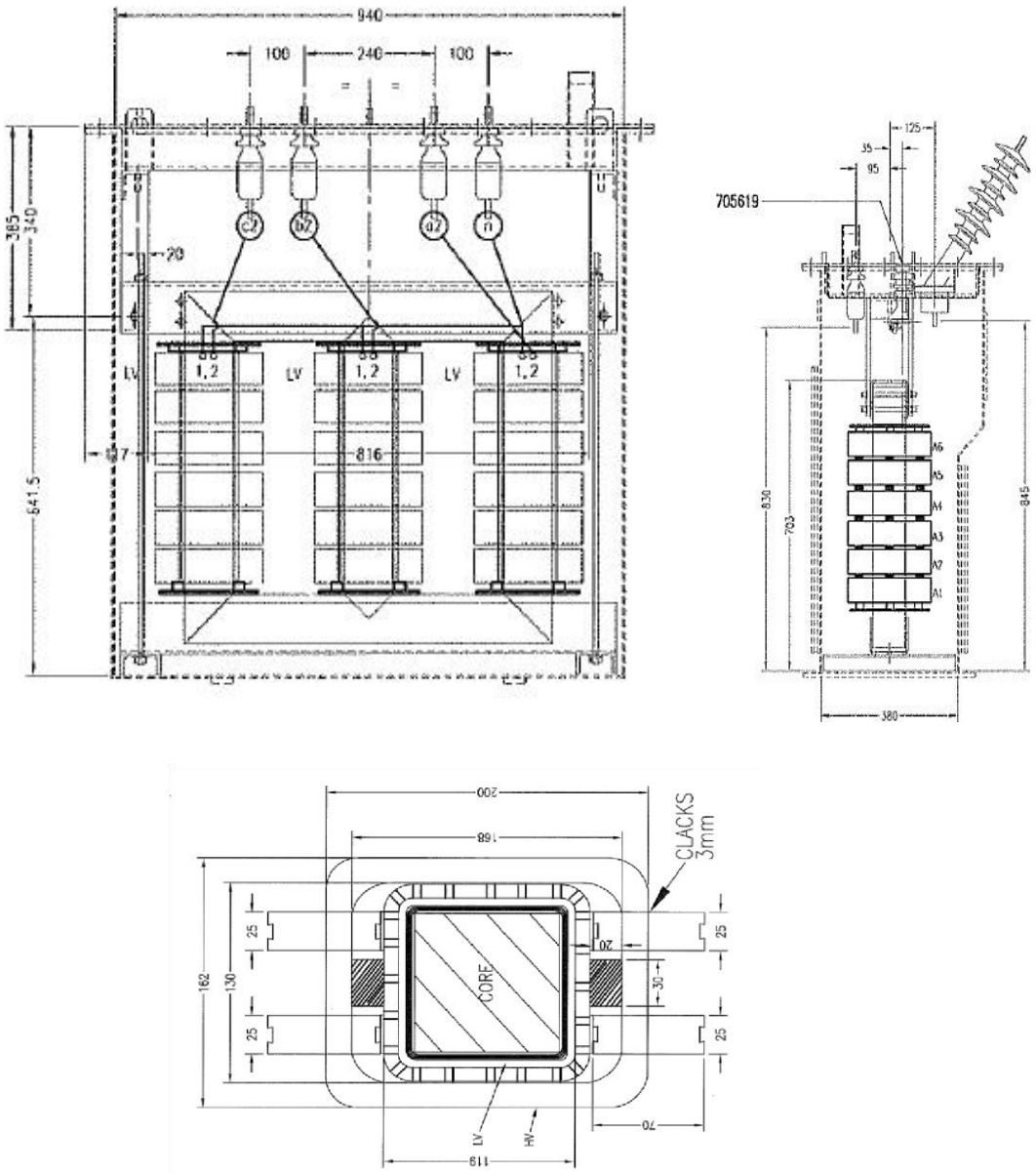

Figure 3.2. Transformer geometrical design details

Using the detailed design data of the transformer, it is modelled in 3D finite element. Figure shows the FEM model of the transformer which consists of core, HV and LV winding, main insulation parts, radial and axial spacers, transformer oil and the tank. The FEM model is built based on the size and material of transformer design PDF.

2) Equivalent Maxwell Spice Circuit

The transformer 3D finite element model shown in Figure 3.4 is then exported into a Maxwell Spice circuit for post-processing to emulate the performance of online IFRA test performed in the laboratory. In this regard, all three phases of transformer HV

winding are energized with 50-Hz power wave travelling through the transformer in its normal operation as a part of the power system. Simultaneously, the LV winding is excited by a controllable nanosecond pulse with an amplitude of 1 kV and duration of 300 ns. Since access to the bushing is limited in online IFRA, the excitation pulse is injected into the LV winding through a 30 pF capacitive coupling mounted on the outer layer of the bushing. which is added to the Spice circuit manually and shown in Figure 3.4.

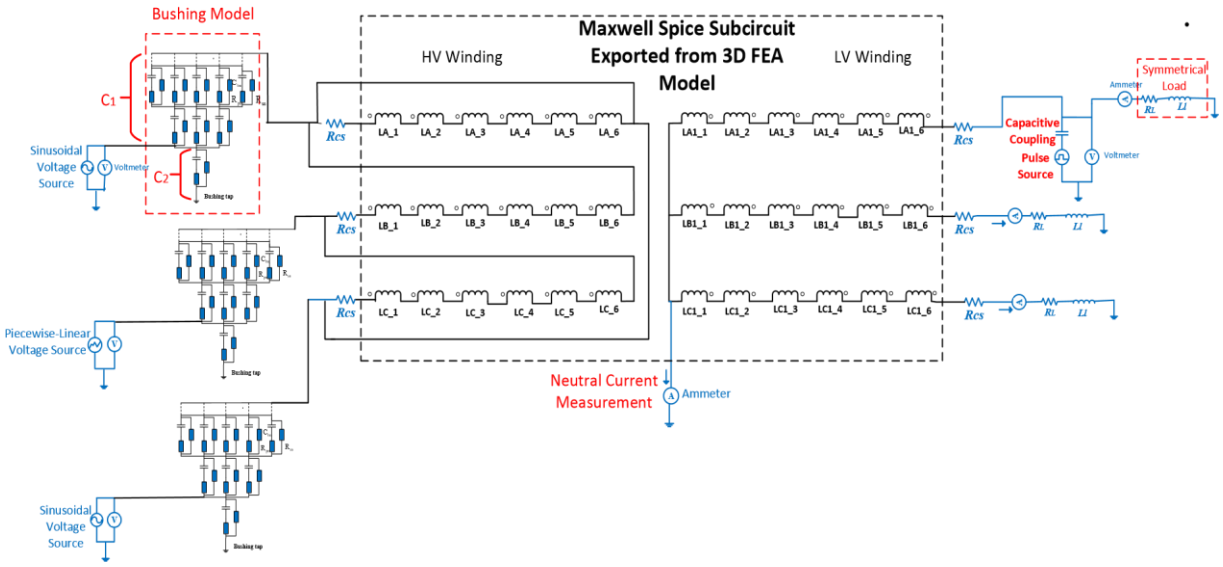

Figure 3.4. Maxwell SPICE circuit

In order to match the real test condition more closely, a bushing model is also manually added to the Spice circuit. . The insulation body of an OIP transformer bushing is comprised of several cylindrical layers of insulation material wound around a central core. The insulation layers are usually filled with an insulating fluid such as oil whose ageing and moisture content have noticeable impacts on bushing dielectric properties. In order to achieve a high degree of uniformity in the electric field, conductive layers are placed between paper layers [39]. The above described construct acts as a set of capacitors connected in series, creating a capacitive voltage splitter. Generally, two capacitances can be measured in bushings, C_1 and C_2. The main insulation system is represented by C_1 which is equivalent capacitance of the inner insulation layers. $C2$ is the capacitance between the measuring tap and the earthed flange and other earthed parts. In the bushing model used in this circuit, the capacitance C_{bn} of each layer can be calculated using equation (3.10), where ε_r is the relative dielectric constant of dielectric material, l_n is the length of n_{th} bushing layer

and r_n is the radius of nth bushing layer. Volume resistance R_{sn} can be obtained using equation (3.11), where ρ is the resistivity and R_{pn} is a resistance in the range of MΩ which represents surface resistance of bushing layers and bushing external insulation dielectric.

$$C_{bn} = \frac{2\pi\varepsilon_r\varepsilon_0 l_1}{\ln\frac{r_1}{r_0}} = \frac{2\pi\varepsilon_r\varepsilon_0 l_2}{\ln\frac{r_2}{r_1}} = \ldots = \frac{2\pi\varepsilon_r\varepsilon_0 l_n}{\ln\frac{r_n}{r_{n-1}}} \tag{3.10}$$

$$R_{sn} = \rho\int_{r_{n-1}}^{r_n}\frac{dr}{2\pi r l_n} = \frac{\rho}{2\pi l_n}\ln\frac{r_n}{r_{n-1}} \tag{3.11}$$

Figure 3.5 shows the 10 kVA bushing modeled in 3D finite element (FEM). The calculated parameters are given in Table 3.2 and 3.3 parameters are given in the table.

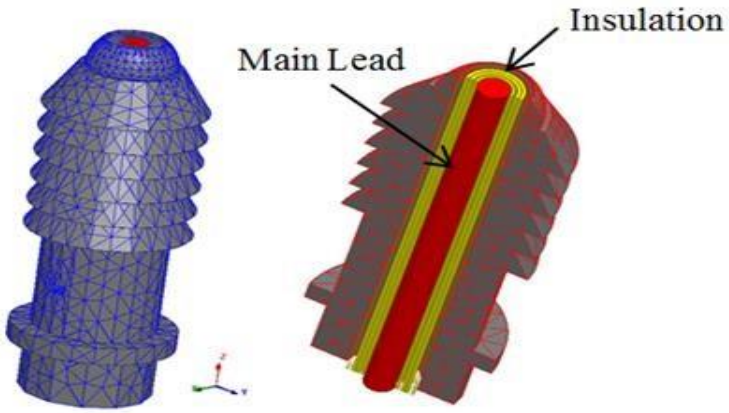

Figure 3.5. 3D model of Bushing solved in electrostatic FEM solver

Table 3.2. Bushing Model Parameters

Electrical parameters	C_1	C_2	L_S	R_S
Value	2000pF	450pF	2.5μH	0.2Ω

Table 3.3. Dielectric properties of bushing

Dielectric properties	Oil	Paper layer	porcelain
ε	2.4	2.5-16	6.5

To construct the transfer function, the output current is measured from the neutral of the LV winding using an ammeter. The input voltage and output current resultant from simulation are shown in Figure 3.6.

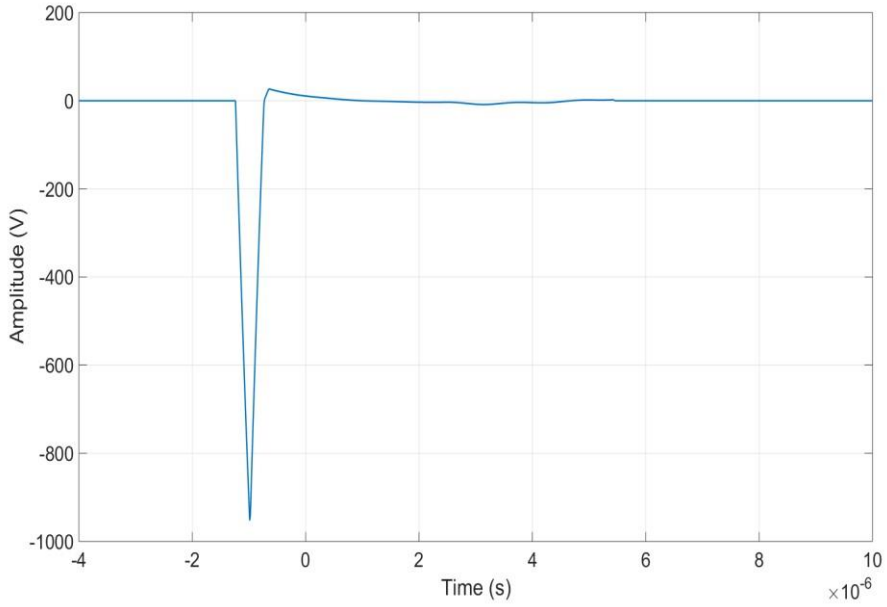

(a)

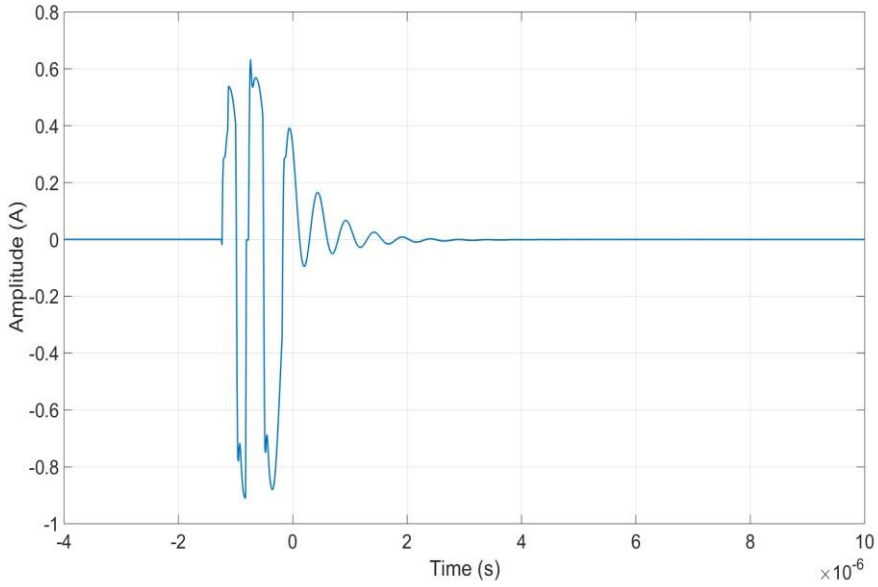

(b)

Figure 3. 6. Simulation signals a) input voltage, b) output current.

B. Case study 2

The same methodology is used for modeling a three-phase 35 MVA, 132kV deltawye connected power transformer shown in Figure 3.7 and calculating its equivalent circuit parameters. The HV and LV windings consist of 9 disks.

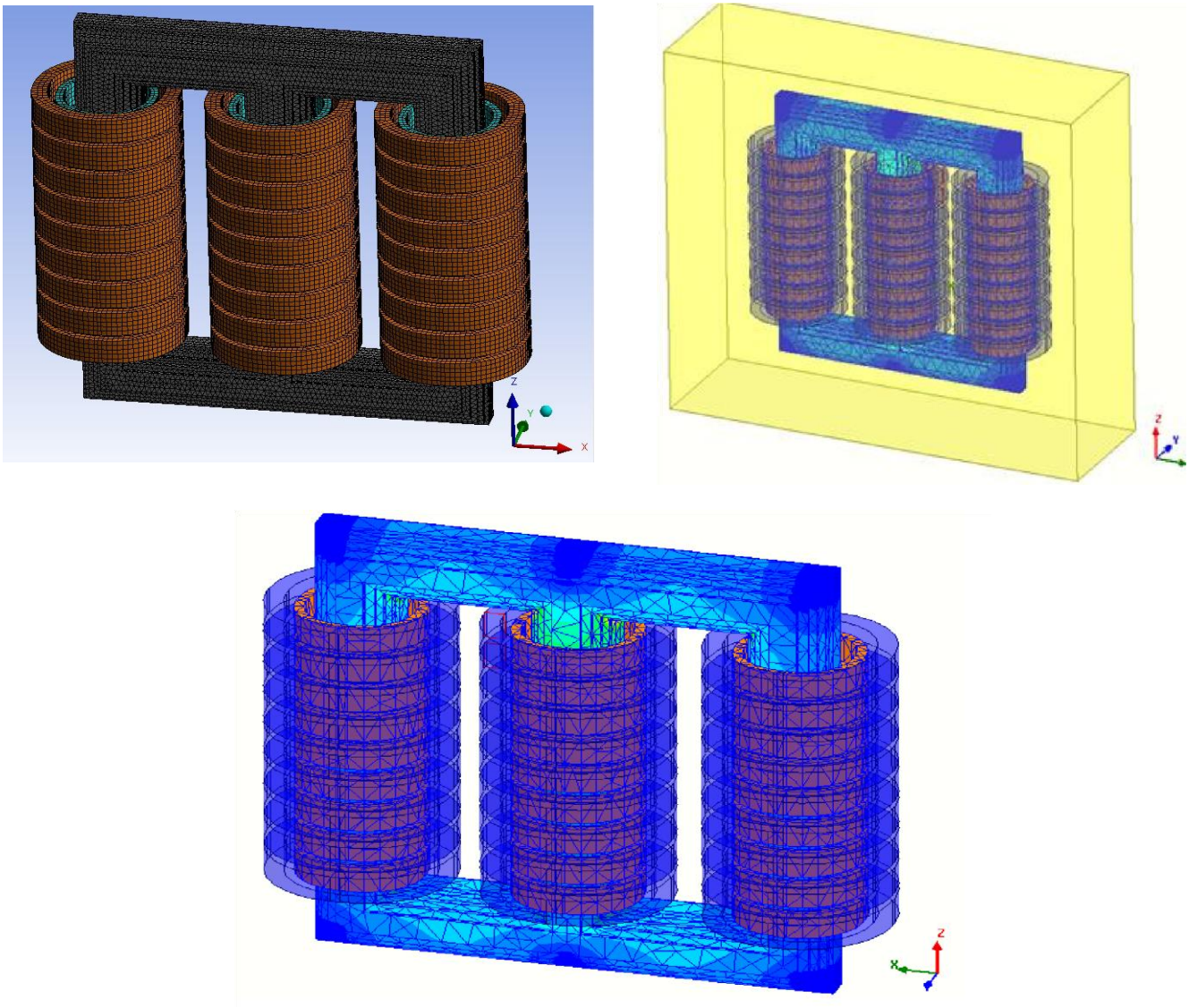

Figure 3.7. Power Transformer 3D model

A volume outside winding is filled with oil (yellow rectangle) for simulating the oil-immersed insulation structure. The relative permittivity and conductivity of mineral oil are set to 2.4 and 10^{-11}S/m respectively in material properties. The cellulose paper insulation can be modelled in FEM as narrow cylindrical layers between LV and HV winding with a relative permittivity of 4 and a conductivity of 1.5×10^{-13} S/m. The transformer 3D finite element model shown in Figure is exported into a Maxwell Spice circuit for post-processing where the test is emulated and the input voltage and output current are measured. The input voltage and the resulting output current are depicted in Figure 3.8.

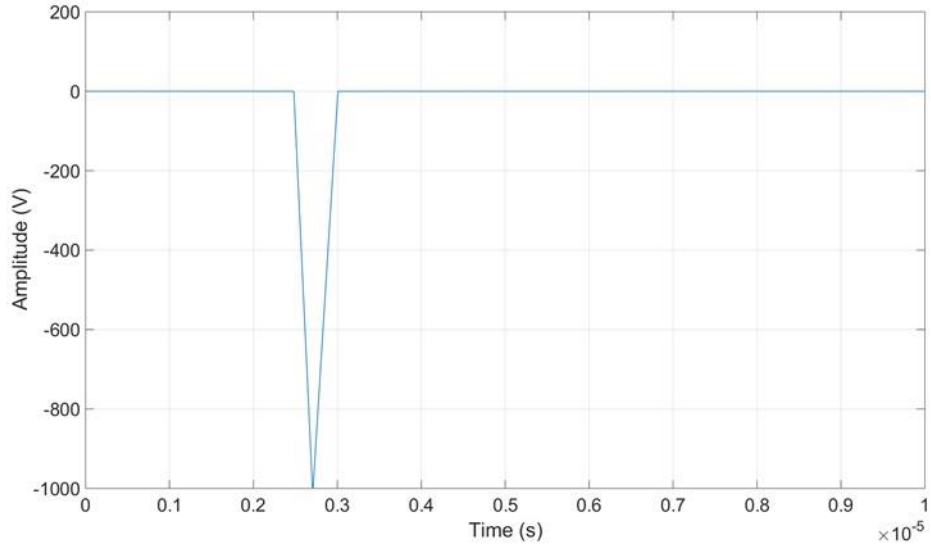

(a)

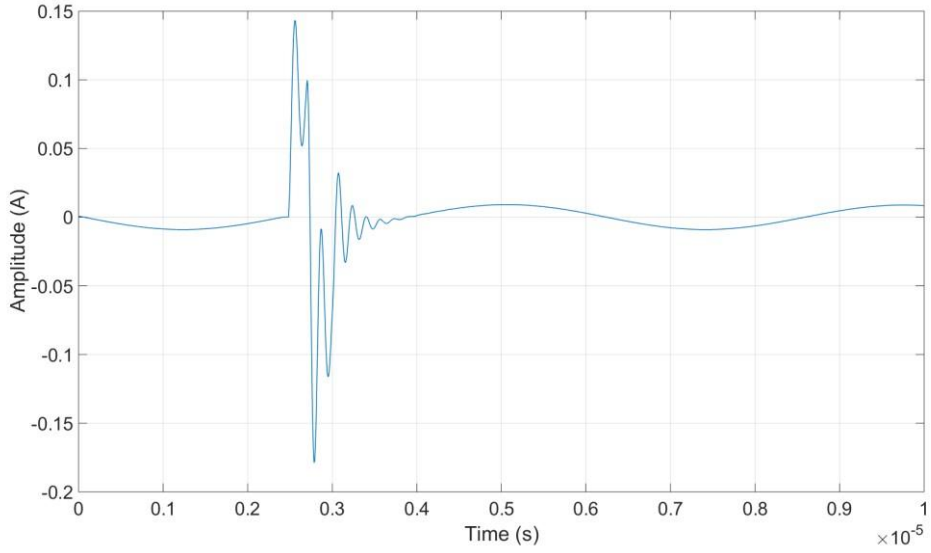

(b)

Figure 3. 8. Simulation signals a(input voltage, b(output current

3.2 Mechanical Fault Simulation

Mechanical stresses caused by caused by assembly configurations, manufacturing malfunctions, eccentric forces, vibration and mainly short-circuit result in transformer winding mechanical faults, including winding deformations and displacements (axial/radial), winding looseness, clamping pressure defects and core defects. In order to determine the impact of mechanical faults on the transformer online IFRA signature, mechanical deformations are imposed on the

3D finite element model of both transformers under study and the response

signal (output current) is measured in faulty conditions. By using the embedded Maxwell Spice in the ANSYS Maxwell package, the effect of mechanical deformations will be automatically considered by exporting the faulty winding in Maxwell Spice and the excess calculations conducted by other studies to determine the percentage change in the parameter values due to different levels of mechanical faults, will not be required.

A. Case Study 1

The 3D finite element model of the transformer is used to emulate the occurrence of mechanical fault in transformer windings. Using the prestress pre-set on the windings and elasticity property of spacer can help predict the dynamic deformation of transformer winding. Since the elasticity property of spacer is far lower than the copper disk, resulting in a more significant deformation in spacers. In this model, both the winding disk and spacer are considered as elastic bodies. 3D FEM is used to analyze the dynamic magnetic-mechanic response considering the influence of prestress from the supporting points. The fixed constraint is pre-set on the interfaces between radial spacers and copper disks. As depicted in Figure 3.9, the maximal displacement appears in the outline of copper disk.

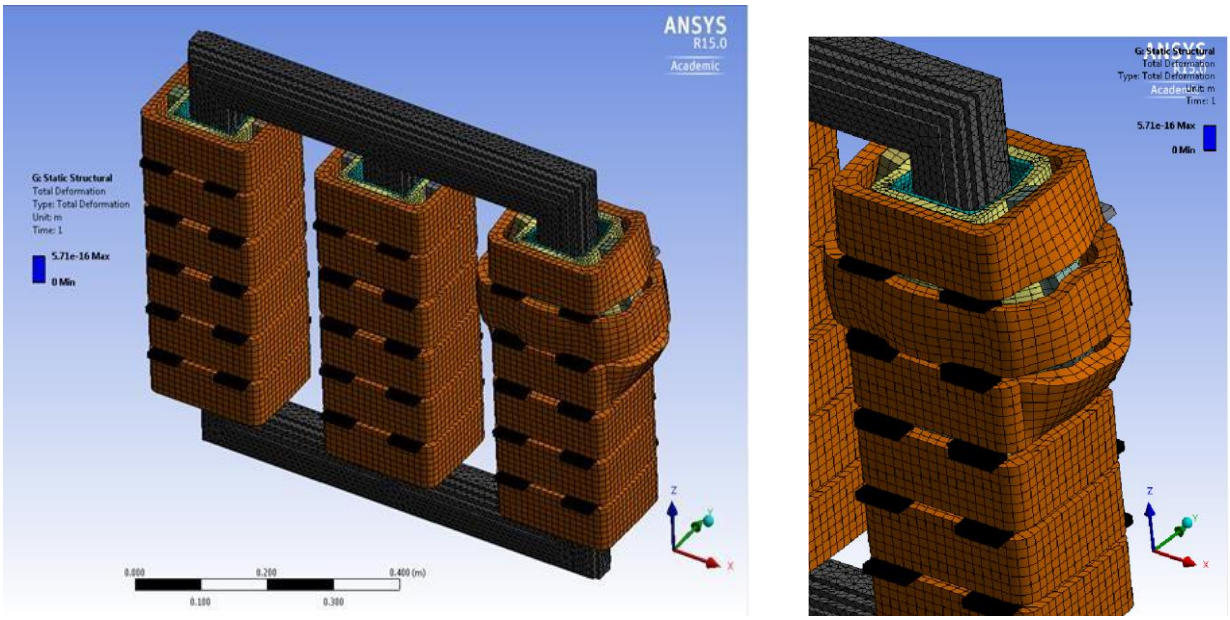

Figure 3.9. 3D finite element model of the deformed winding

B. Case Study 2

In concentric windings, the current passing through the winding produces a magnetic flux with radial and axial components. The interaction between the axial component of the flux and the winding current produces repulsive radial forces between HV and LV winding. When exceeding the material elastic limit of the spacers located in axial direction, these forces lead to radial deformation in the inner winding (forced buckling) and the outer winding (hoop buckling). To investigate the impact of hoop buckling on online transformer IFRA signature, radial deformation has been imposed on the transformer FEM model as shown in Figure 3.10. The deformed FEM model is then exported into the external Spice circuit and the output current is recalculated for the faulty condition.

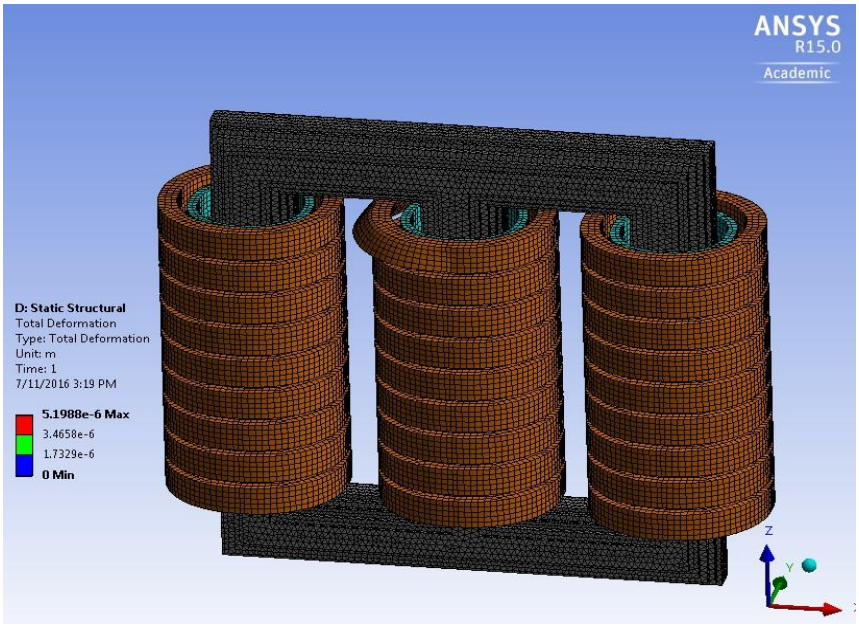

Figure3.10. Free buckling deformation

3.7 Simulation of Noise and External Interferences

The ingress of external interferences affects the sensitivity and reliability of the acquired test data. In order to achieve an acceptable level of reliability and get a repeatable measure not influenced by external factors, it is required that the impact of potential external interferences on the transformer online FRA test be determined. In this section, firstly, the potential external interferences which could cause distortion in this particular online test are identified. Secondly, the methodology through which the coupling of external interferences with the results obtained from

the online IFRA test is emulated is discussed. Analysis of the obtained results and how they affect the transformer IFRA signature will be discussed in Chapter 4.

3.7.1 Noise Characteristics

In online IFRA test, major external interferences which can be troublesome for the measurement and assessment of the results are wide-band noises which can be classified as stochastic noise and white noise as tabulated in Table 3.4. Other types of noise including harmonic distortion and discrete spectral interference

(DSI) are considered narrow-band noises which, if present, will only appear at a very limited area of the signature and will not affect the whole signature trend, nor will they result in false judgement of transformer internal condition. Therefore only the two former types are considered in the de-noising process presented in Chapter 5.

Stochastic noise is considerably difficult to remove due to its similarity with the impulse signal used as excitation voltage for transformer IFRA test. Background noise is the most common type of noise present during online measurements of transformers. It possesses a flat power spectrum with equal power at all frequencies.

Table 3. 4 TYPES AND CAUSES OF NOISE

Type of noise	Causes of noise	Noise Category
Pulse-shaped interferences from the power system	Switching operations Lightning strokes Arcing between adjacent metallic contacts PD and corona	Stochastic noise
Background noise (e.g. thermal)	Ambient Test setup	White Gaussian Noise

3.7.2 Noise Simulation Method

3.7.2.1 External pulse-shaped Interferences

Using Maxwell Spice as the external circuit allows for modelling the noise Pulseshaped interferences which ingress from the power grid inside the transformer winding. In order to detect the impact of the first type on the transformer IFRA test, the input voltage of one of the phases in the equivalent Spice circuit of the transformer shown in Figure 3.4 is switched from a pure sine wave to a signal with voltage spikes and voltage notches using a Linear Piecewise type voltage source which can have values of voltage assigned to it at each time step. Figure 3.11 a and b depict the characteristics of the signals being fed to the transformer from the power grid in these cases.

Since the excess voltage due to imbalances in each of the three phases of the transformer goes through the neutral of the transformer, in the case that the current going through the neutral point of wye-connected winding is being measured as the output signal of the test, the does not necessarily have to happen at the phase on which the IFRA test is being conducted.

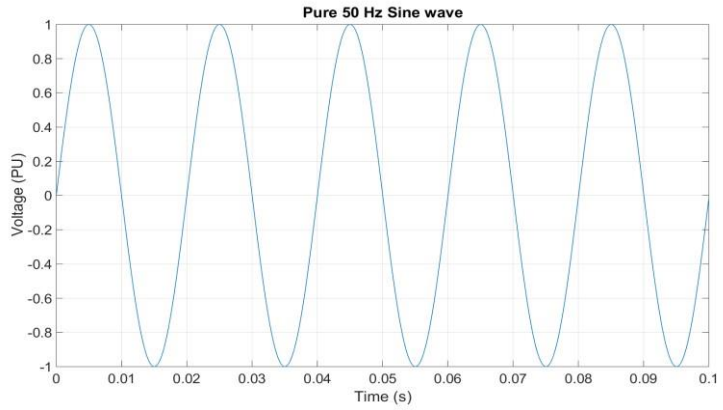

(a)

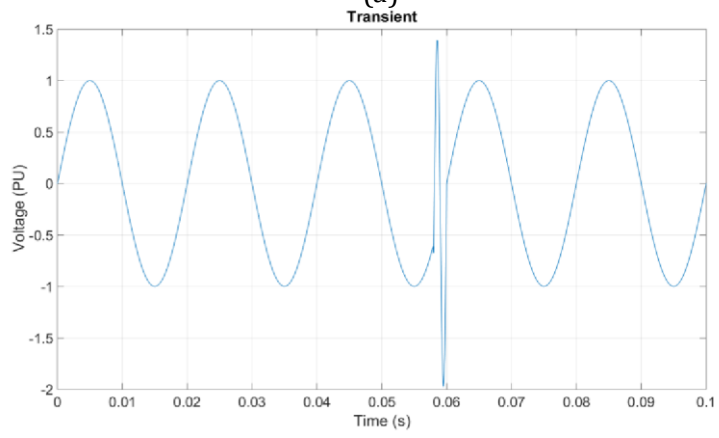

(b)

Figure 3.11. Input voltage a) pure sine wave b) switching transient

3.7.2.1 Internal pulse- between shaped Interferences

The occurrence of partial discharge (PD) activity in oil-immersed transformers is the prominent indicator of insulation deterioration, which if not detected in incipient levels can lead to further damage resulting in transformer failure. Although on-site PD measurements have been extensively discussed in the literature, the impact of partial discharge on transformer frequency response analysis has not been elaborated.

Internal partial discharge between different sections of the winding is imposed on the model under study in order to determine its impact on the online IFRA test. To this end, a current pulse signal simulating the PD reported in [41] with a front time of 10 ns, fall time 30 ns and amplitude of 50 mA is injected between the inductances representing disk 2 and 3 of the LV winding in the Spice circuit and the output current is measured. Figure 3.12 shows the variation of the output current of the transformer as a result of internal pulsive discharges between adjacent winding sections.

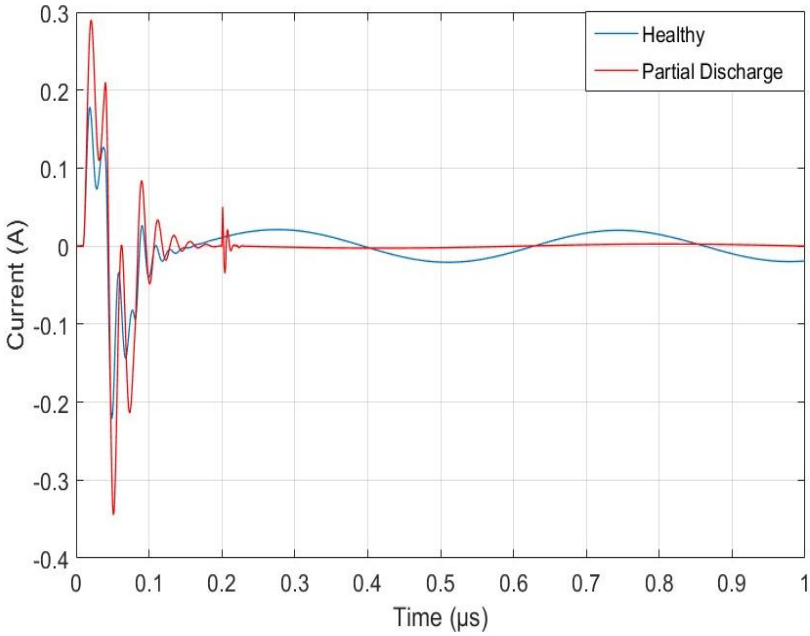

Figure 3.12. Output current variation internal partial discharge vs normal condition

The pulse signal simulating the PD acts as an additional source exciting the winding which explains the rise in the amplitude of the response. In the presence of PD, a number of new resonance and anti-resonance appear in the transformer signature in <600 kHz frequency range which corresponds to the oscillations appearing in the

impedance frequency characteristics as a result of partial discharge propagation in the winding [41].

3.7.2.1 Background Noise

For modelling background noise, White Gaussian Noise with signal to noise ratio (SNR) of 45 is added to the measured output signal signals in Matlab. Figure 3.13 shows the output current measured in simulation coupled with the additional white Gaussian noise.

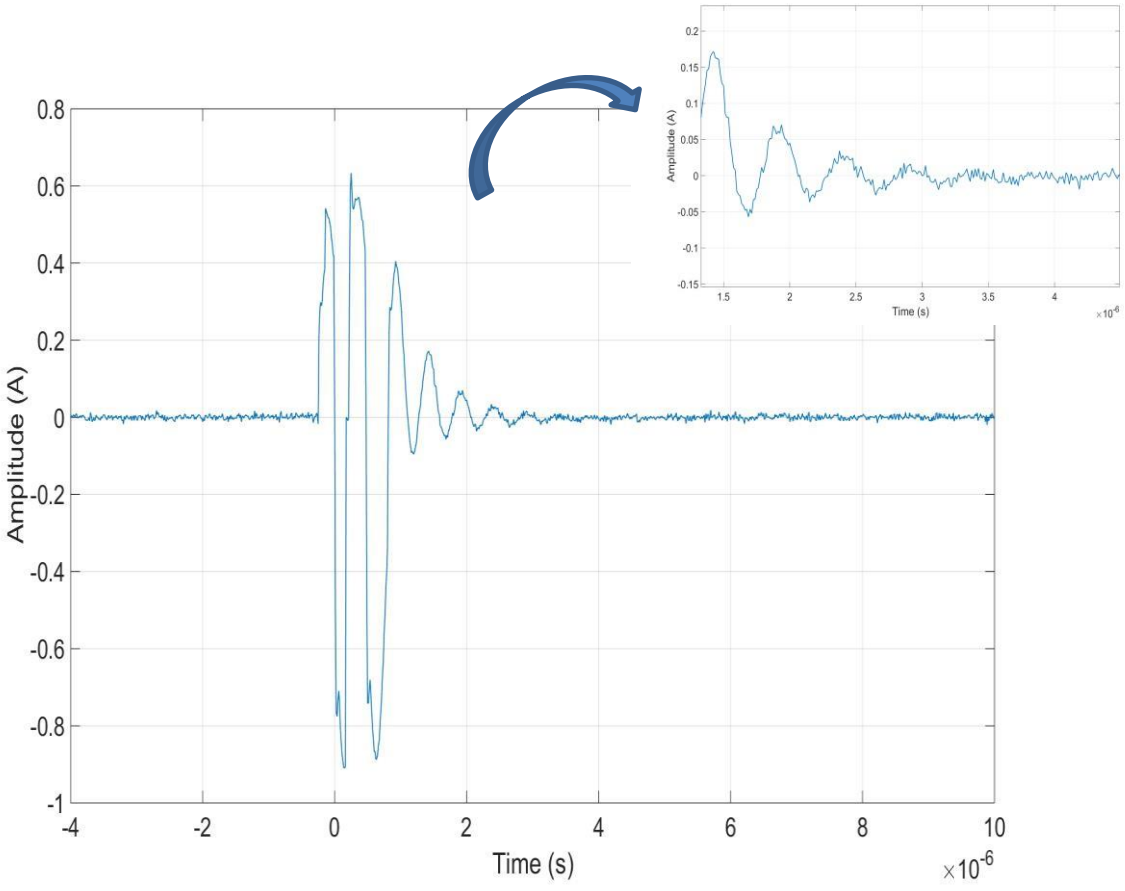

Figure 3.13. Background noise added to output current

4. Signal Processing

4.1. Introduction

Mathematical processing is applied signals in the domain of time to determine their frequency content and construct the FRA curve. The common tool used by the majority of operators for the mathematical procedure is the fast Fourier transformation (FFT). However, FFT is not the best choice since this tool is useful for processing stationary signals since it only provides the frequency content of the signal with no information on the time each frequency component has occurred.

In [32] the use of continuous wavelet transform (CWT) is proposed to overcome the non-repetitive effects and nonactual resonant behaviour of the FFT. The multi-resolution analysis embedded in wavelet transform has the capability to retain both the frequency content and the time information of the signal. To be able to classify both high and low frequency phenomena, however, it is required to use additional neural networks and FFT calculation routines in conjunction with the wavelet transform [33], which in turn, leads to a heavier computational burden.

On the other hand, the S–transform [42] as an extended version of wavelet transform. The s transform utilizes a moving and scalable localizing Gaussian window to approximate different parts of the signal with features superior to both the Fourier and Wavelet transforms. The S transform is capable of being completely converted from the one-dimensional time spectrum to the twodimensional t-f (time-frequency) and from there to the well-known frequency domain i.e. Fourier domain. Bothe the magnitude of time-frequency and phasefrequency spectra can be used to determine the local characteristics of the signal. The superiority of the S transform with respect to Wavelet and Fourier transforms stems from the fact that the sinusoidals it uses are fixed in timedomain while the window (e.g. Gaussian/ Hyperbolic window depending on the type of S transform being used) is being moved and scaled. Therefore, because the phase spectrum is always referred to the static reference point of the time axis origin, it will be absolute. The real and imaginary components of the signal can thereby be localized according to the basis function under study and useful information can be extracted by following the changes that take place in the absolute phase of a given frequency. This property within the S transform enables an improved

power quality disturbance transient detection and localization since it entails a phase correction of the Wavelet transform.

4.2 Generalized S Transform

The S transform is a tool for mathematical processing of signals which provides features of both the Wavelet transform and short-time Fourier transform simultaneously. The disadvantage of having the same analysing window for all frequencies in STFT is that because it lacks the capability of accommodating various cycle scales of various frequencies, it suffers from low resolution for low and high frequencies. This issue can be resolved by the modification of the STFT to let its windows be scaled with the change of frequency, as the ones in wavelets do. For a time variable signal h(t), the Continues Wavelet Transform
(*CWT*) is computed by equation (4.1) given in [43]:

$$CWT(\tau, a) = \int_{-\infty}^{+\infty} h(t) w(\tau - t, a) dt \tag{4.1}$$

where, is the mother wavelet, α and τ are scaling and translating parameters, respectively. The S-transform is a modified wavelet transform. The S-transform of the time variable signal *h(t)* can be defined as a *CWT* with a Gaussian wavelet used as its mother wavelet and also multiplied by a phase factor, as below:

$$S(\tau, f) = \int_{-\infty}^{+\infty} h(t) \left\{ \frac{|f|}{\sqrt{2\pi}} dt \times \exp\left(\frac{-f^2(\tau - t)^2}{2} \right) \times \exp(-2\pi i f t) \right\} dt. \tag{4.2}$$

where, *S* is the S-transform of the function *h(t)*, τ defines the position of the mother wavelet function over the time-axis and f denotes the frequency. The
Gaussian window of (4.2) is substituted with a generalized window to drive Generalized S-transform, as follows[43]:

$$S(\tau, f, p) = \int_{-\infty}^{+\infty} h(t) w_G(\tau - t, f, p) \exp(-2\pi i f t) dt. \tag{4.3}$$

In equation (4.3), p is a set of parameters controlling the window shape.

4.3 Hyperbolic S Transform

Generally, among two windows of the same duration, a better resolution is provided when using an asymmetrical window compared to a symmetrical one and therefore, at low frequency conditions where the frequency resolution is less critical a hyperbolic window (asymmetrical) is used. However, with the increase of frequency, the window's shape changes towards a Gaussian window which is symmetrical. For deriving the hyperbolic S transform, the Gaussian window within the generalized S transform is substituted by a hyperbolic window as follows [44]

$$w_H = \frac{2|f|}{\sqrt{2\pi}(\gamma_f + \gamma_b)} \times \exp\left\{\frac{-f^2\left[X(\tau - t, \{\gamma_{HY}^B, \gamma_{HY}^F, \lambda_{HY}^2\})\right]^2}{2}\right\} \quad (4.4)$$

and X is defined, as follows:

$$X(\tau - t, \{\gamma_f, \gamma_b, \lambda_H{}^2\}) = \left[\frac{\gamma_f + \gamma_b}{2\gamma_f\gamma_b}\right](\tau - t - \zeta) + \left[\frac{\gamma_f - \gamma_b}{2\gamma_f\gamma_b}\right]\sqrt{(\tau - t - \zeta)^2 + \lambda_H{}^2} \quad (4.5)$$

In equation (4.4), X is a hyperbola in which depends upon a backward-taper parameter, a forward-taper parameter (we assume 0<° *FHY* <° *BHY*), and a positive curvature parameter which has units of time. ζ is a translation factor which ensures that the peak of hyperbolic window happens at $\tau - t = 0$. ζ can be obtained as follows:

$$\zeta = \sqrt{\frac{(\gamma_f - \gamma_b)^2 \lambda_H{}^2}{4\gamma_f\gamma_b}} \quad (4.6)$$

In (4.5), the optimal value of forward and backward for each signal can be defined so that the best the most energy concentration and the best time-frequency resolution is achieved.

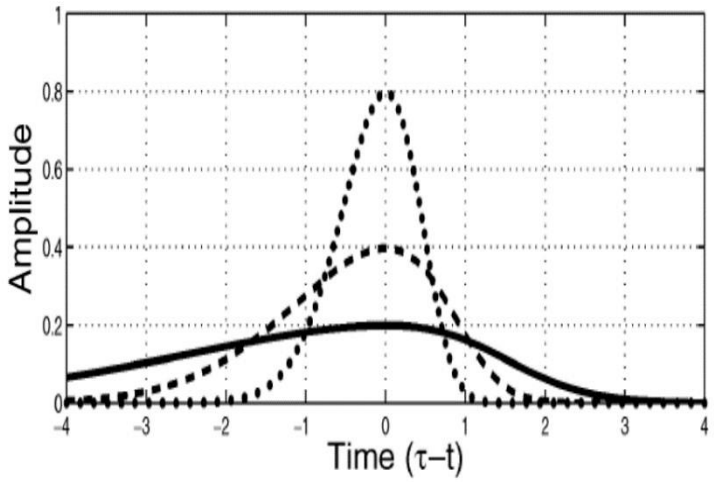

Figure 4.1. Variation of hyperbolic window with different frequencies [45]

As a result of the close relation between the FFT and the S transform, the Fourier transform can be used to define the discrete S transform [42]. The average over all values of τ would then give the FFT of the signal as

$$S[n, j] = \sum_{m=0}^{N-1} H(m+n)\mathrm{G(m, n)}\exp(\mathrm{i}2\pi\mathrm{mj}) \tag{4.7}$$

In this equation the parameters n ,m and j vary from 0 to N-1, where N is the number of the samples in the signal. *H(m+n)* denotes the discrete Fourier transform *H(m)* shifted along the frequency axis. The output of the S transform of a signal is a *M×N* matrix which contains complex values. The rows of the output matrix represent the signal frequencies and its columns show the signal samples. The S matrix's energy (E) is defined as [46]

$$E = \mathrm{Re}\,al\left\{ \sum_{j=1}^{N} \sum_{i=1}^{M} [(\mathbf{SMAT} \times \mathbf{SMAT}^{*})]_{ij} \right\} \tag{4.8}$$

The electrical impedance of the winding can be calculated based on the energy ratio between input and output signals.

$$|Z_a| = \sqrt{\frac{E_{OutputCurrent}}{E_{InputVoltage}}} \tag{4.9}$$

Takin advantage of S transform, enables control over both time and frequency axes i.e. time-frequency contours, which can be used as a complementary tool for assessment of IFRA test results.

4.4 Application of HST in the Detection of Abnormalities

4.4.1 Case Study 1

A) Winding Mechanical Deformation

The process of imposing mechanical deformation on transformer winding is explained in the previous chapter. Figure 4.3 shows the impact of winding internal mechanical fault on transformer online IFRA signature and the time-frequency contour of the output current.

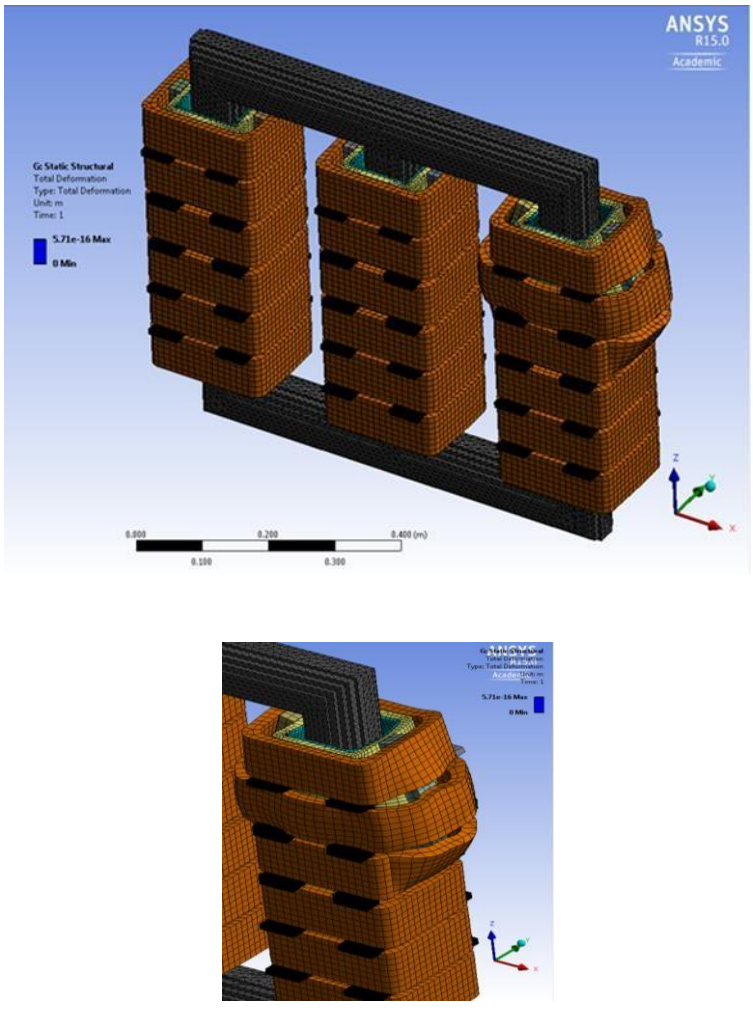

Figure 4.2. 3D finite element model of the deformed winding

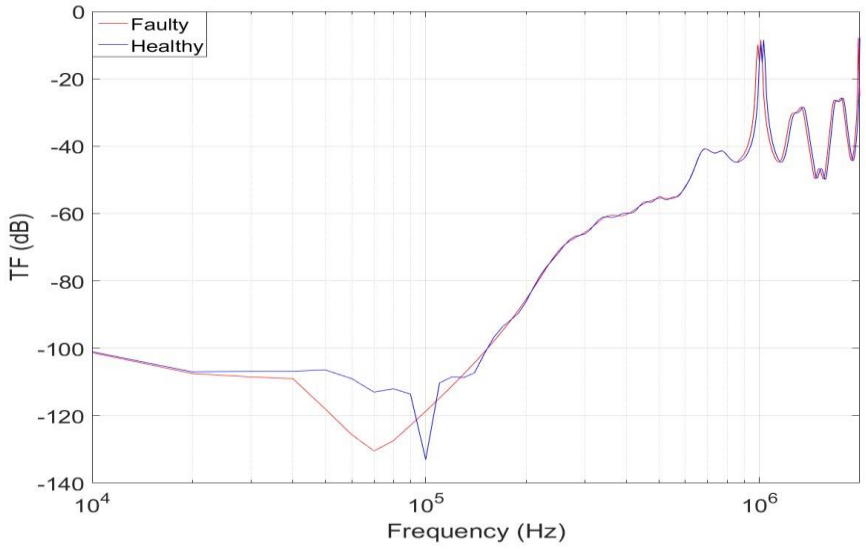

(a)

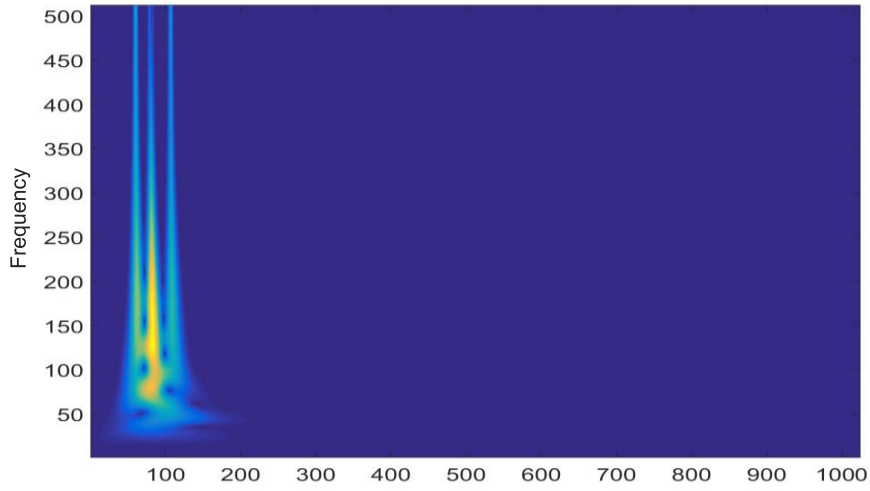

(b)

Figure 4.3.The impact of internal mechanical fault on a) transformer online IFRA signature b) time-frequency contour of the output current.

B) Winding Mechanical Deformation

In order to detect the impact of the first type on the transformer IFRA test, the input voltage of one of the phases shown in figure 3.11 is switched from a pure sine wave to a signal with voltage spikes and voltage notches. Figure 3.11 shows the characteristics of the signals being fed to the transformer from the power grid in these cases. By manipulating the time of the switching occurrence, it can be adjusted so that it occurs simultaneously or with a short delay with respect to the IFRA excitation pulse signal but still within the sampling time. The IFRA signature in both these cases will vary from the no-noise condition similarly. However, taking advantage of time-frequency contours, these two cases can be differentiated. Figures 4.4 and 4.5 show the impact of external switching transients on the derived IFRA

signature and time frequency contours. In the case shown in Figure 4.4, the transformer with healthy internal condition is used.

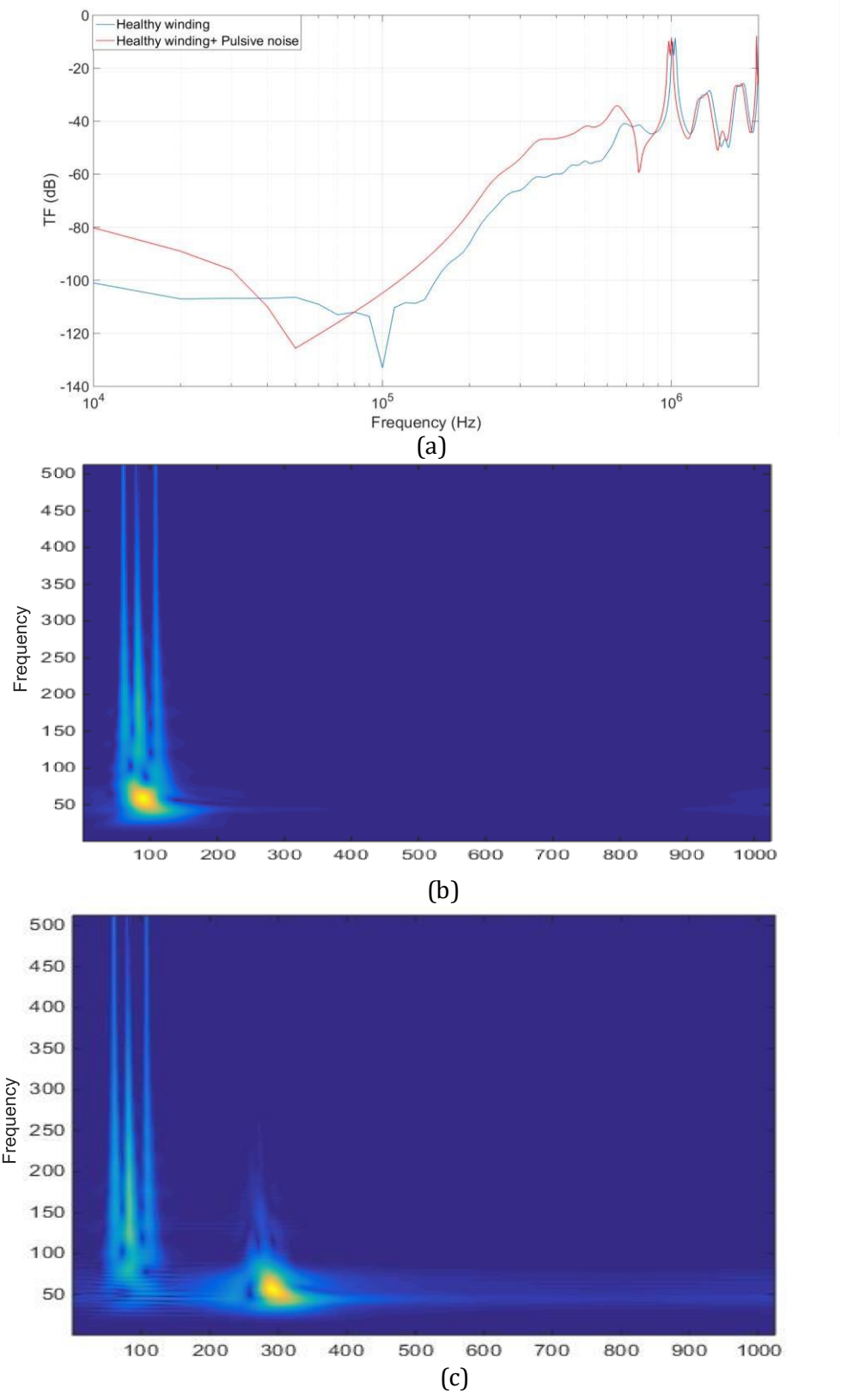

Figure 4.4. The impact of external pulsive noise on healthy winding a) transformer online IFRA signature b) time-frequency contour of the output current in the simultaneous event of external pulse with IFRA impulse c) time-frequency contour delay between external pulse and IFRA impulse.

Figure 4.5 depicts a condition with same external interferences as the former case with the difference that the transformer winding is mechanically deformed as in Figure 4.2.

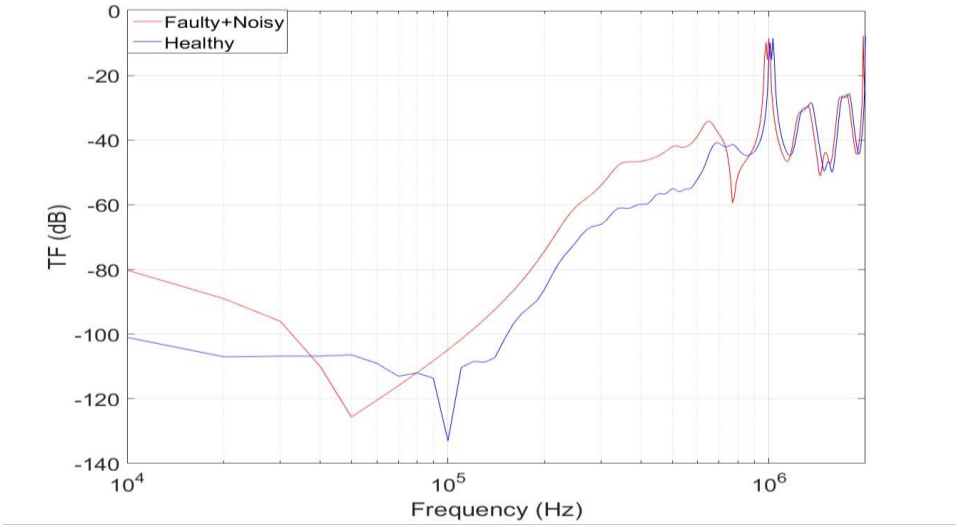

(a)

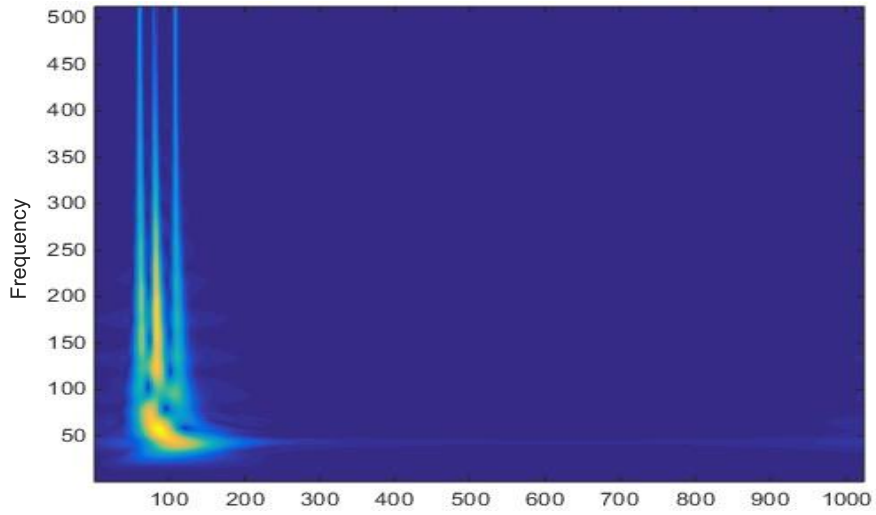

(b)

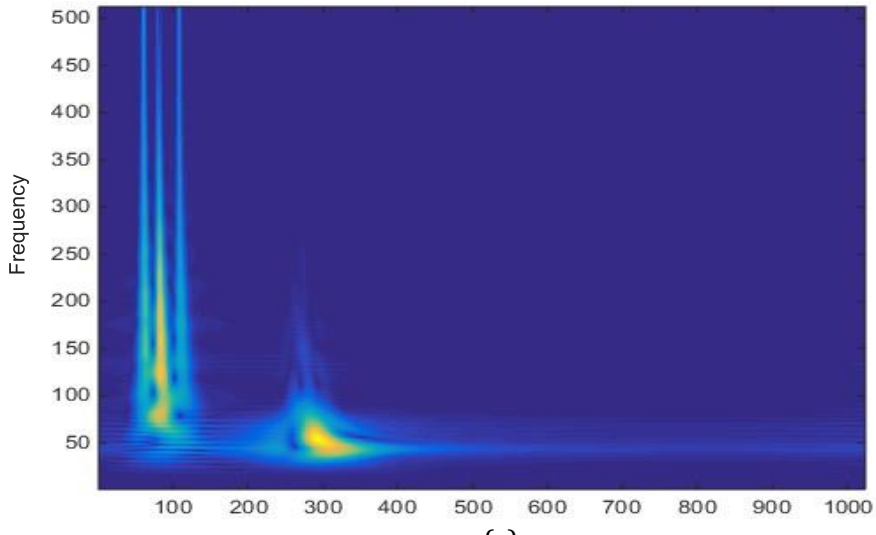

(c)

Figure 4.5. The impact of external pulsive noise on winding with internal mechanical fault a) transformer online IFRA signatu re b) time-frequency contour of the output current in the simultaneous event of external pulse with IFRA impulse c) time frequency contour delay between external pulse and IFRA impulse.

IFRA signature and output current time-frequency contour which is illustrated in Figure 4.6.

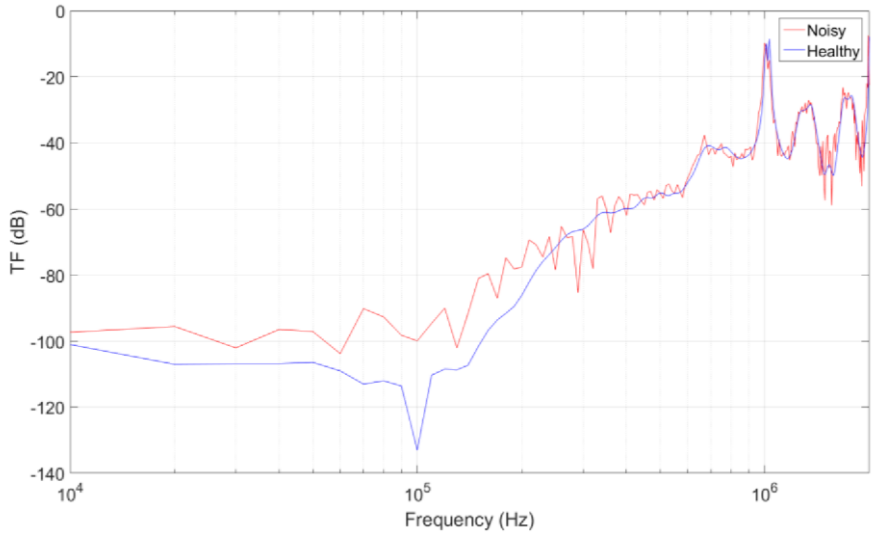

(a)

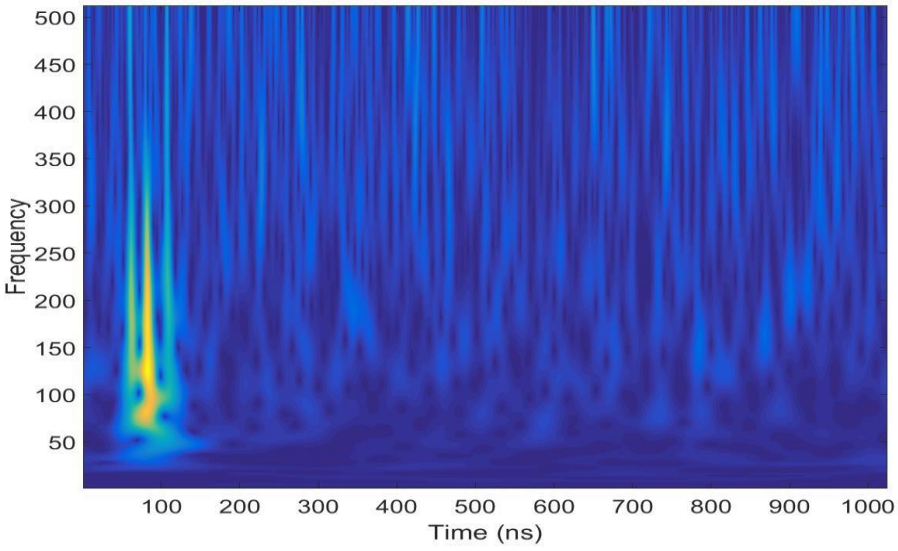

(b)

Figure 4.6.The impact of background noise on a) transformer online IFRA signature b) time-frequency contour of the output current.

4.4.2 Case Study 2

A) Internal Partial Discharge

Figure 4.7 shows the impact of internal pulsive discharges between winding sections on the results obtained from signal processing of the IFRA test signals on the second transformer under study which is shown in Figure 2.7.

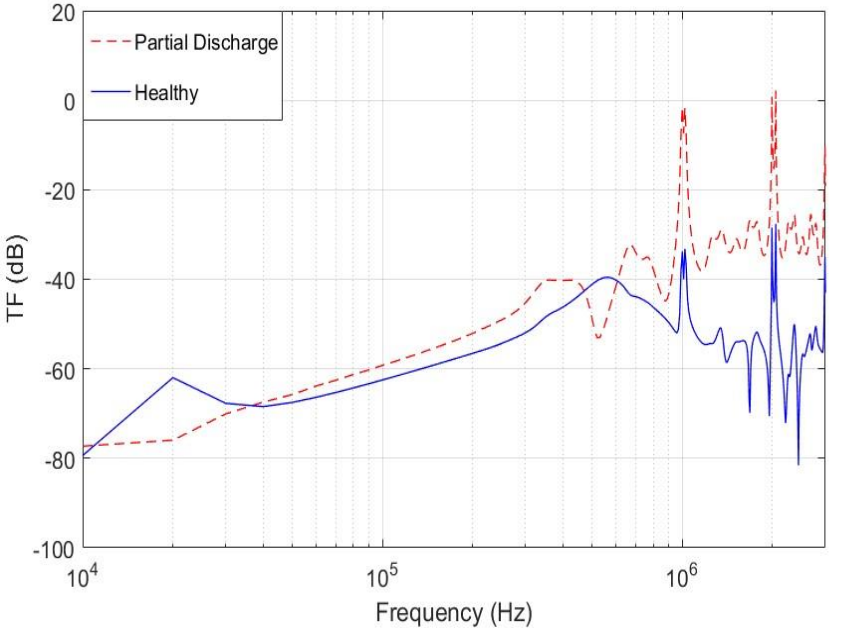

(a)

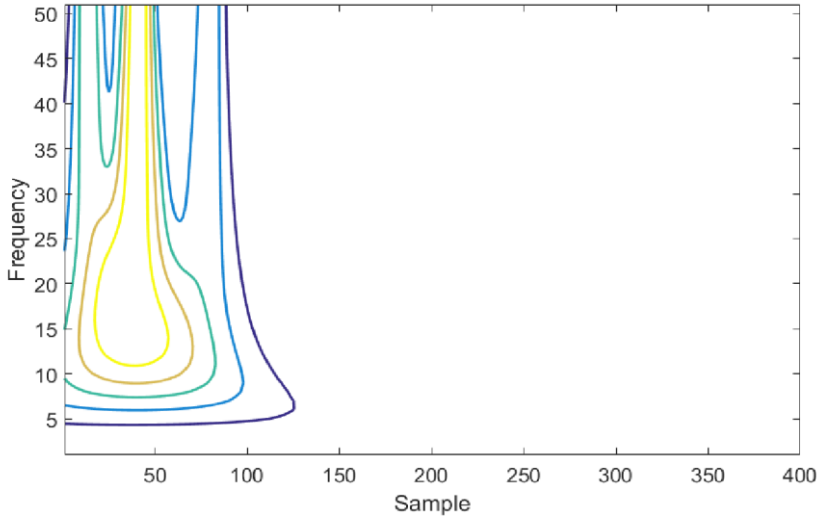

(b)

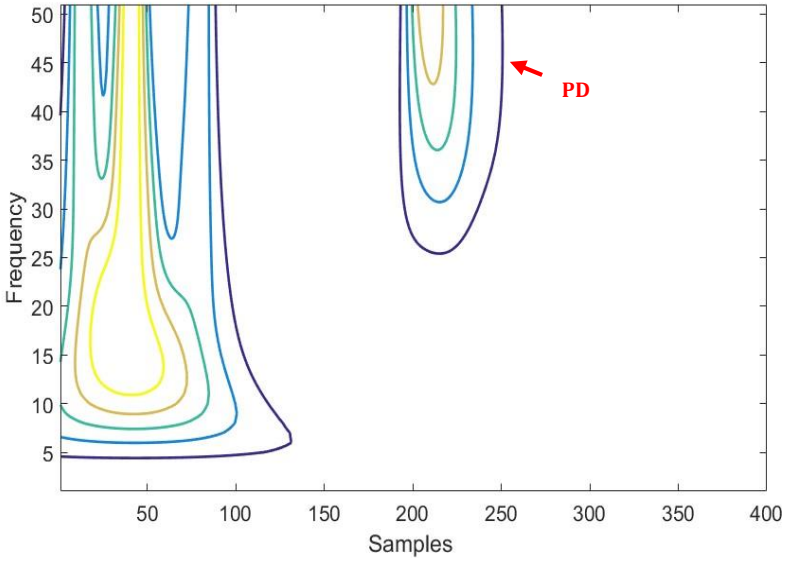

(c)

Figure 4.7. a) Variation of IFRA signature b) Time-frequency contour of the output current in normal condition c) Partial discharge between winding sections

B) Free Buckling

Transformer online IFRA signature as well as the time frequency contour of the output signal in the case of buckling deformation on transformer outer winding as shown in Figure 4.8 (a) are plotted and depicted in Figures 4.8 (b) and (c), respectively.

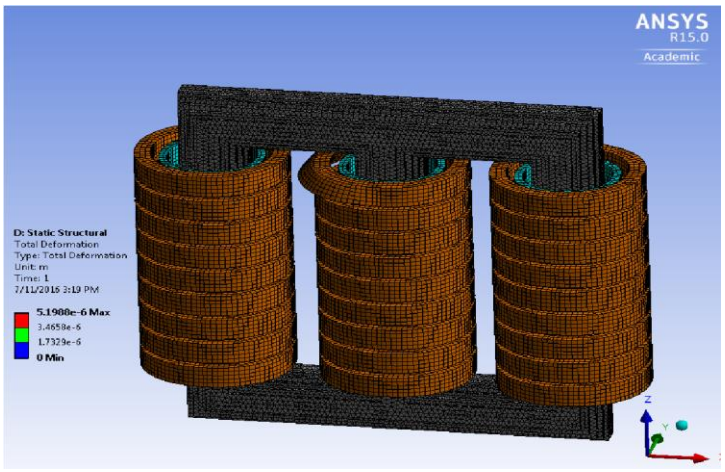

(a)

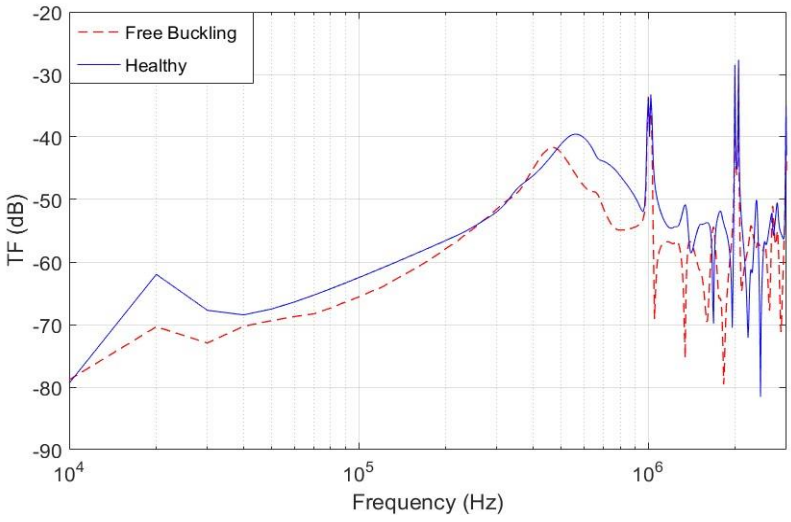

(b)

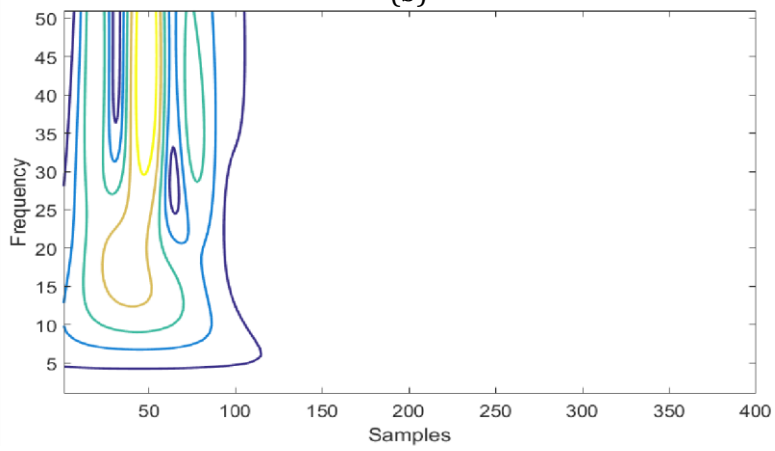

(c)

Figure 4.8. Free buckling deformation (a) Online IFRA signature (b) Time-frequency contour of the output current

As a result of free buckling in the transformer winding, a shift of resonant and anti resonant frequencies is observed in the whole frequency range with respect to the healthy condition As a result of buckling deformation the existing spike in the time frequency contour in the healthy condition alters, which outlines the aforementioned shift in the position of resonance and anti-resonance. However, as opposed to the first condition, where a new spike representing the PD pulse signal was added to the time- frequency contour of the output current, in this case no noticeable change is witnessed in the time axis.

5. Filtering Technique

5.1. Introduction

Due to the shortcomings of the available frequency domain techniques, interest has been generated towards developing time-frequency filtering methods as an alternative. These filters are applied to the t-f distribution of a signal instead of the familiar Fourier spectrum. Such two-dimensional distribution can be achieved by using the S transform, which is a modified version of STFT with scalable windows moving alongside the frequency axis, similar to those of wavelets. It has recently been shown that the local spectra of the S transform have equivalents in time domain. The requirement of a filter varying with time can be made clear by taking advantage of Figure 5.1. This figure shows the timefrequency distribution of a synthetic signal, which is comprised of two sets of time series: a noise component and a signal component, with the former being shown in grey and the latter in black. Designing a filter for such a signal should be carried out in a manner that it removes the noisy part while leaving the signal component intact; a filter that blocks the noise component and passes the remainder of the signal i.e. the signal component. Since the cut-off frequency of a proper filter for this job needs to be different at different points in time, it is required that a filter whose cut-off frequency changes with time be used. The characteristic of this type of filter can be defined as a t-f weighing function, M (t, f), which is effectively '1' over the regions containing the real signal and '0' over the regions that contain noise components.

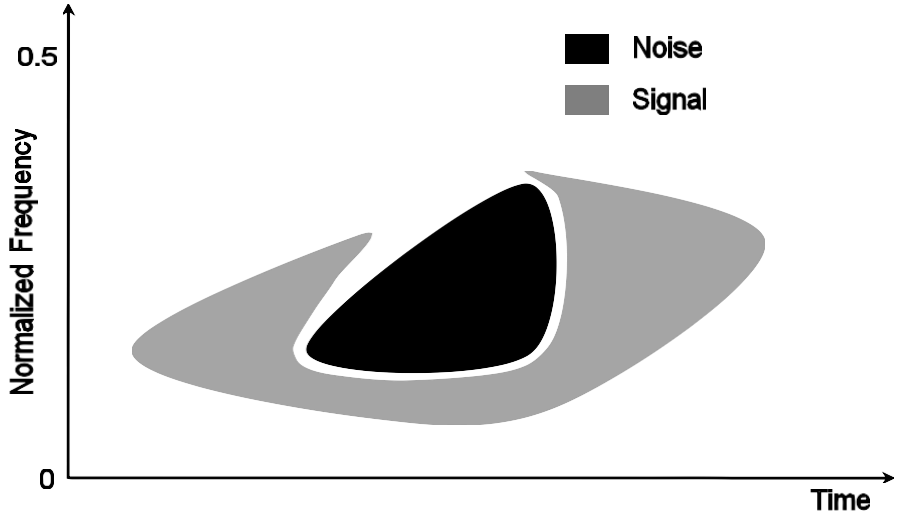

Figure 5.1. Need for linear time variant filters [46]

5.2 Filter Design

The time-frequency filter designed in this study for retaining the FRA signature of the transformer inherent to its internal mechanical condition and not influenced by external interferences, is obtained using the healthy signature of the transformer. As shown in the previous chapter, the occurrence of fault does not result in deviation of the time frequency contour in time-frequency axes. Alternatively, it changes the intensity of the healthy contour in certain areas depending on the kind (axial/radial) and intensity of the fault. This change is shown in the contour by a more highlighted color. Therefore the filter obtained using the healthy signature of the transformer will not eliminate the impact of fault, but merely eliminates the fingerprints outside its time-frequency representation, which are in essence the fingerprints of external interferences and noise.

To design the time-frequency filter, firstly, Matlab is used to compute the M×N matrix obtained from the hyperbolic S transform of the healthy winding. Secondly, this matrix is converted to an intensity image which containing values in the range of 0.0 (black) to 1.0 (full intensity/white). By specifying a threshold value in the range of [0,1], the grayscale image can be converted to a logical (black and white) image which is in essence the filter mask used to filter out the noise.
There parameters which can be manipulated while designing the filter include

- Forward taper γ_f and backward taper γ_b value defining the shape of hyperbolic window

- The threshold value of converting the intensity image to the filter mask

The optimal value of forward and backward for each signal can be defined so that the best the most energy concentration and the best time-frequency resolution is achieved. For this study, the parameter settings for backward and forward tapper was obtained from a sensitivity analysis and set to to 1.36 and 2.3, respectively. The threshold value for converting the grayscale image to the logical image is set to 0.3. Figure 14 shows the intensity image and the logical image obtained in Matlab which works as the filter.

In order to design the filter, firstly, Matlab is used to convert the hyperbolic S transform output of the healthy winding which is a M×N matrix to an intensity image shown in Figure 5.2. In the case that a range is not pre-defined by the user for minimum and maximum intensity, zero (black) will be assigned to the minimum value of the matrix and the maximum value of the matrix will be represented by 1 (white).

Figure 5.2. Intensity image derived from transformer output current time frequency contour

Secondly, by specifying a threshold value in the range [0,1], the grayscale image is converted to a logical (black and white) image which is in essence the filter mask used to filter out the noise. By replacing all the pixels present in the input image, the output (BW image) the pixels which have a luminance greater than the threshold level with the value 1 (white, full intensity) and the ones with a lower luminance with the value 0 (black). The threshold value is the critical point in this part. Figure shows the variation of the derived filter (logical image) as a result of different threshold levels.

(a)

(b)

(c)

Figure 5.3. Time frequency filter mask used for filtering time-limited band-limited noise with threshold value of a) 0.38 b) 0.3 c) 0.22

The threshold for the logical image is 0.3. The logical image is the filter mask.
The contour is converted to a picture then the areas of the picture of are drawn.

5.3 Obtaining the Filtered Response

As discussed in the previous chapter, discrete S transform can be obtained by modifyig the short discrete Fourier transform (STFT) by using a hyperbolic window (which scales with frequency) instead of the fixed analyzing window in STFT as following [43],

$$S[\tau, f] = \sum_{t=0}^{N-1} h[t]\, \omega[\tau - t, f] \exp\left(\frac{-2\pi i f t}{N}\right) \qquad (5.1)$$

Implementing an inverse DFT of (5.2) will then give the inverse S-transform,

$$h[t] = \frac{1}{N} \sum_{f=-N/2}^{N/2-1} \sum_{t=0}^{N-1} S[\tau - t, f] \exp\left(\frac{2\pi i f t}{N}\right) \quad (5.2)$$

The latter expression is important since the the inverse S transform is the basis based on which time-frequency filtering becomes possible. In order to implement time-frequency filtering, S in (5.2) can be multiplied by a user-defined timefrequency filter F. The filter F in this study is the matrix containing the data from the logical image in Figure 5.3. Substituition of the product $S \square F$ instead of S then gives a filtered time series $h^F[t]$ given in (5.3) [47]

$$h^F[t] = \frac{1}{N} \sum_{f=-N/2}^{N/2-1} \sum_{t=0}^{N-1} S[\tau - t, f]\, F[\tau, f] \exp\left(\frac{2\pi i f t}{N}\right) \quad (5.3)$$

The product of the S transform surface and the filter mask eliminates the noise signatures from the signal. By taking an inverse S transform of the new S transform plane using (5.3) gives the filtered signal.

5.4 Verification of the Proposed Filtering Technique

Figure 5.4 (a) and (b) show respectively the time-frequency contour and IFRA signature and of a case study used to evaluate the effectivity of the proposed denoising technique. In this case study the mechanically-deformed signature of the transformer is obtained in the presence of both background and pulsive noise. The filtering technique is then applied to this signal and the same results are shown after filtering and de-noising. As can be seen the impact in Figures 5.5 (a) and (b), by using the designed filter the impact of noise has been removed to a large extent from the transformer frequency response while the impact of fault still remains on the signature. This shows that proposed filtering technique does not have the common problem in greedy de-noising techniques which is the elimination of useful data in addition to the noise and can be used as a step before assessment of the online IFRA test signals.

The proposed algorithm can be used as a block before assessment of the transformer internal mechanical condition so that the pulse-shaped interferences propagating inside the transformer winding from the power system and background noise coming from the measuring device and ambient does not result in misinterpretation

of the results which could, in turn, lead to unnecessary costs for disconnecting the transformer from the power grid because of fault alarms.

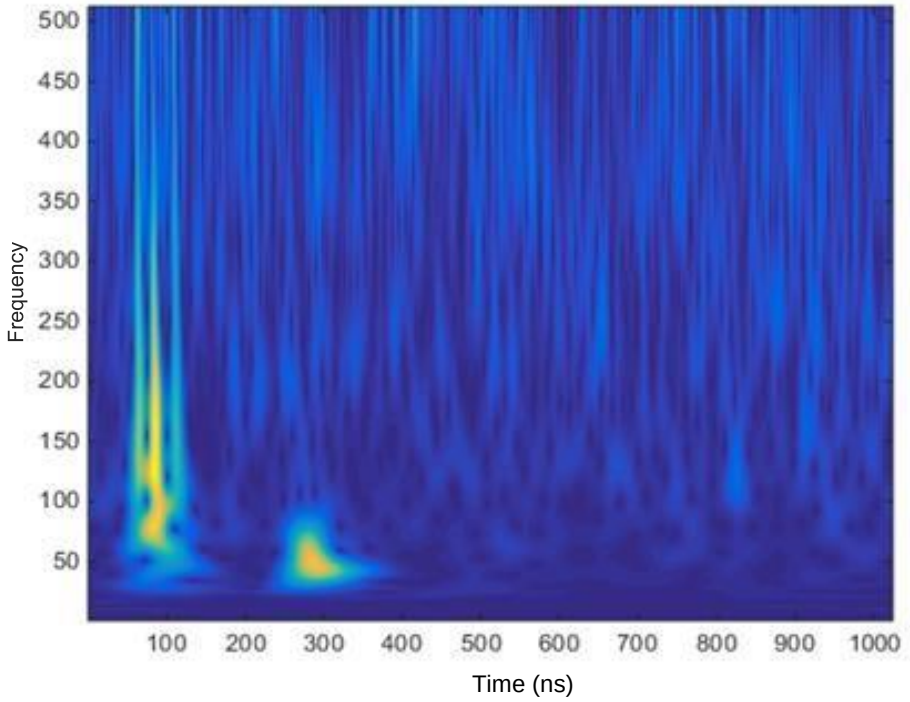

(a)

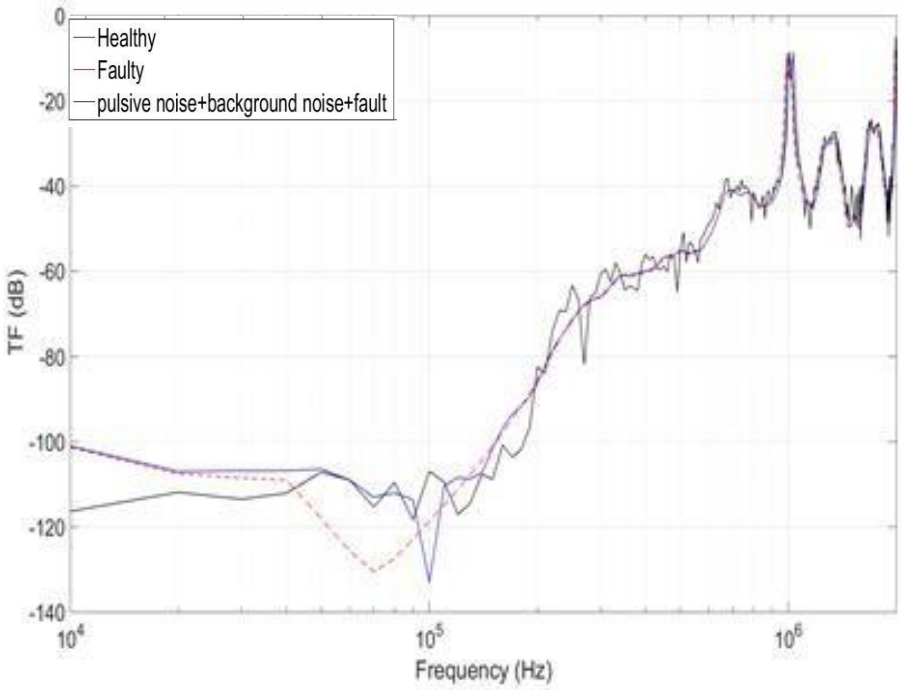

(b)

Figure5.4. Faulty winding in the presence of background and pulsive noise a) transformer noisy online IFRA signature b) time-frequency contour of the output current in the noisy condition

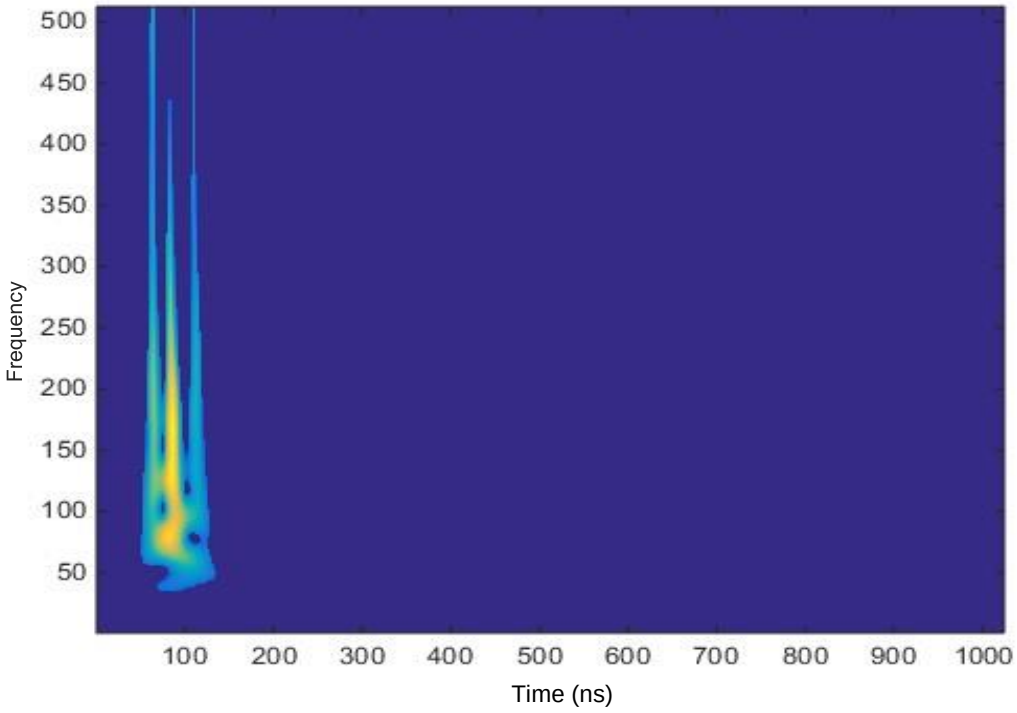

(a)

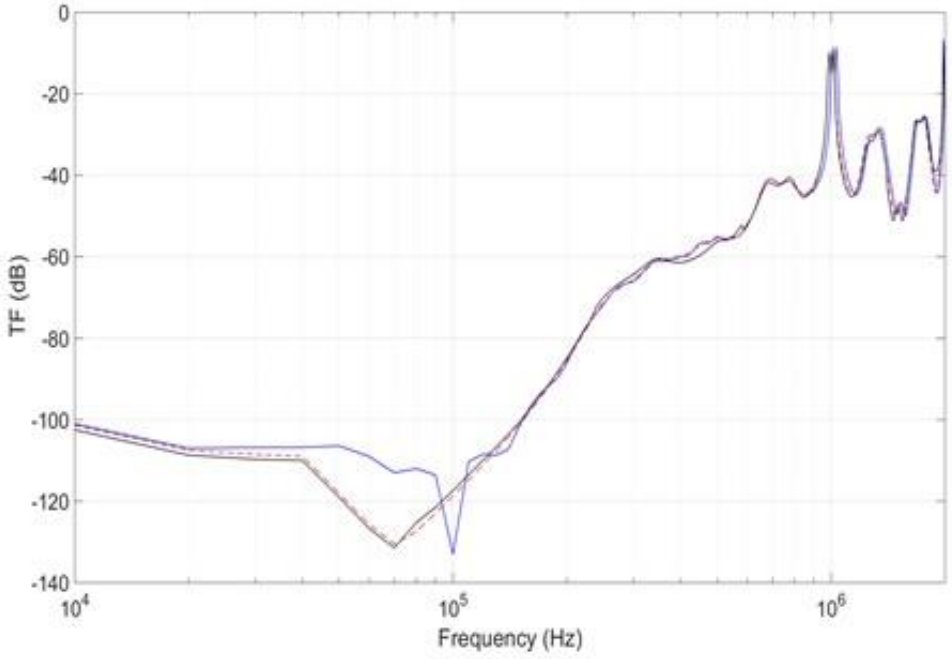

(b)

Figure 5.5. a) time-frequency contour of the output current after filtering implementation b) filtered transformer online IFRA signature

6. Experimental work on online IFRA method

6.1 Introduction

As offline FRA has been in widespread use for years now, a significant amount of work has been done in the domain of offline testing [11-13], which requires the transformer to be isolated from the system and taken out of service to conduct the test. Offline FRA, therefore, is more of a corrective approach implemented after the occurrence of faults and is hardly sufficient for preventing failures. To address this issue resolve this problem, online performance of the frequency response technique has recently piqued interest among the scientific community. Performing the test online while the transformer is in non-stop service enables the detection of fault signs at very early stages and prevents forced outages with consequential losses [4, 5]. Two methods exist for implementing FRA, impulse frequency response analysis (IFRA) and sweep frequency response analysis (SFRA). A majority of the available literature have opted for IFRA for online application [3, 17].

A number of studies and contributions have been made for the implementation of the frequency response test while the transformer is in service [8-10] which involves injecting controllable pulses on top of the 50/60 Hz power passing through the transformer winding while the transformer is energized working as a part of the power system. Depending on the size of the transformer, the pulses are injected through either bushing tap or a non-invasive coupling circuit placed on the outer layer of the transformer bushing. The response signal is also measured using a coupling circuit or a Rogowski coil [16, 21]. In [10] developed a basic online transformer test system, in which signals of high-frequency content are injected to the bushing tap of a 650 kV transformer. In [39], Vahid Behjat et al proposed the installation of non-invasive capacitive sensors (NICs) on the bushing surface as an interface to feed the alternating output voltage of their network analyser to the transformer winding and Rogowski coils to measure the output phase currents. Mehdi Bagheri et al [13] suggested adding an impedance in parallel to the bushing tap so as to decrease the level of the voltage induced on the test tap when it is not grounded whilst online testing procedure. In the study devoted by Zhao et al, pulses with controllable Characteristics are generated using a nanosecond pulse generator and then fed as to the transformer winding via a capacitive coupling circuit to excite the natural resonance and anti-resonance of the transformer winding and obtain the

IFRA signature. The response signal is also measured using a bushing capacitive coupling. In [18] how the bushing capacitive coupling circuit affects the online impulse frequency response signature is investigated. The experimental work conducted in this study is based on the methodology proposed by Chenguo Yao et al [50]. Online measurements were performed in of Western Power high voltage laboratory.

6.2 The configuration of the system

The transformer online IFRA test system, which is, in fact, a high-power network analyzer, is comprised of five major elements: a signal generator, a high-power driver, a bushing connection circuit, filters, and a data-acquisition system.

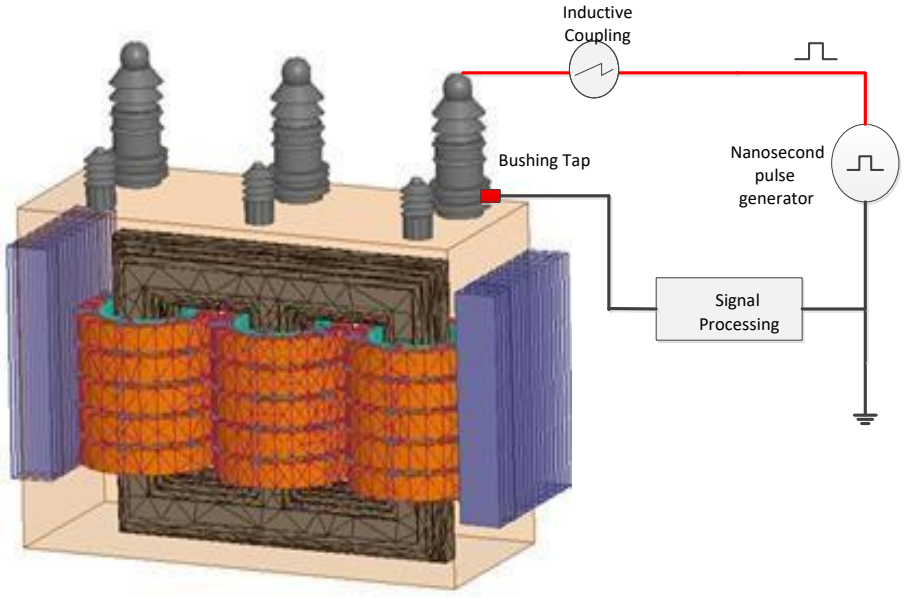

Figure 6.1. Test schematic configuration

6.2.1 Nanosecond pulse generator

Generating controllable repeatable high frequency pulses is imperative to the implementation of online IFRA. As a result of the requirement of a wide frequency bandwidth. Due to the bandwidth, standard CTs and VTs voltage and cannot be used.

In this study the high voltage pulse generator shown in Figure 6.2 is used to generate nanosecond pulses to excite the winding under test.

The generator enables setting the amplitude, width of the generated pulses, utilizing the circuit shown in Figs. 2 and 3. generating controllable repetitive pulses with

sufficiently high voltage amplitude (up to 8 kV), 200 to 1000 ns pulse width, with various resistive loads ranging from 50 to 1000 Ω.

Figure 6.2. Nanosecond impulse generator

The generator is comprised of different parts including a dc charging power, a solid-state Marx circuit with MOSFETs, load and a control circuit.

6.2.2 Signal injection and protection circuit

In online IFRA transformer is energized working as a part of the power system and therefore, access to the winding is limited. Because of its insulation prerequisites, it is a high-cost and complex job to make connections directly from the high voltage bus to the transformer terminal and hence the need for an alternative approach. The majority of high voltage transformers have a bushing tap which, due to the bushing capacitive division features, if used, can induce a far lower voltage level on the terminal of the transformer. To inject controllable pulses with nanosecond duration into the internal winding a capacitive coupling sensor (CCS) mounted on the outermost layer of the bushing, which is, in essence, a metal element on the bushing outer layer, is used [24].

Figure 6.3. Capacitive coupling mounted on bushing

The high-voltage signal is injected to the busing tap via an injection and protection circuit which serves as a pathway with a low impedance for either of the 60-Hz current coming from the power grid and the circuit elements by limiting the voltage exerted on the bushing tap and protect the bushing against rushes of current in case of a circuit failure. The signal protection circuit is made up of the filtering circuits' resistive and capacitive components, denoted as R and C which work as a filter, a tube for discharging additional gas (G) and a Varistor (K) which together serve as overvoltage protection elements. The protection circuit must be designed in a manner to be all-pass in forward direction (while passing through from the pulse generator to CCS) and provide a high impedance path in reverse direction (while passing in the opposite direction) to protect the generator from the over-voltage transients in the power system and 50 Hz frequency power system voltage. The circuit is put in an aluminium box to be protected against external noise and interference. The designed signal injection and protection circuit is shown in Figure 6.4.

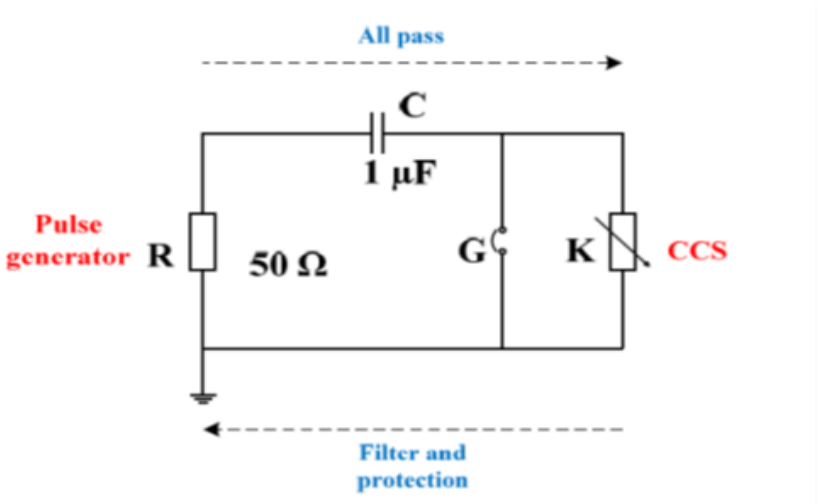

Figure 6.4. Signal injection and protection circuit [50]

6.2.3 Capacitive coupling sensor and capacitive voltage divider

As the output signal of the transformer, the current running from the neutral to the ground of the lv winding of the transformer was measured using a Rogowski coil shown in Figure 6.5. Most transformers in use have at least one wyeconnected winding and therefore, the neutral current of their star winding can be measured as the output signal. Alternatively, in the case of no delta connection, the response signal can be measured using a capacitive voltage divider installed on a different phase of the same winding i.e. instance, when testing phase A of the lv winding, A phase bushing is used to inject the input signal into. The system response can then be measured using a capacitive voltage divider installed on the bushing of lv winding phase C.

Figure 6.5. Signal injection and output measurement

Figure (6.6) shows the setup of the experiment. An experimental test setup was designed and built in order to obtain the response signal operational frequency and characteristics of the capacitive voltage divider. The test initiatory setup is presented in Figure 6.6. For the sake of recording the test waveforms, Tektronix DPO4054 Oscilloscope which has good quality recording capability was used.

6.3 Experimental Results

6.3.1 Offline Impulse Frequency Response Test

Figures 6.9 (a) and (b) show the input voltage and output current measured from

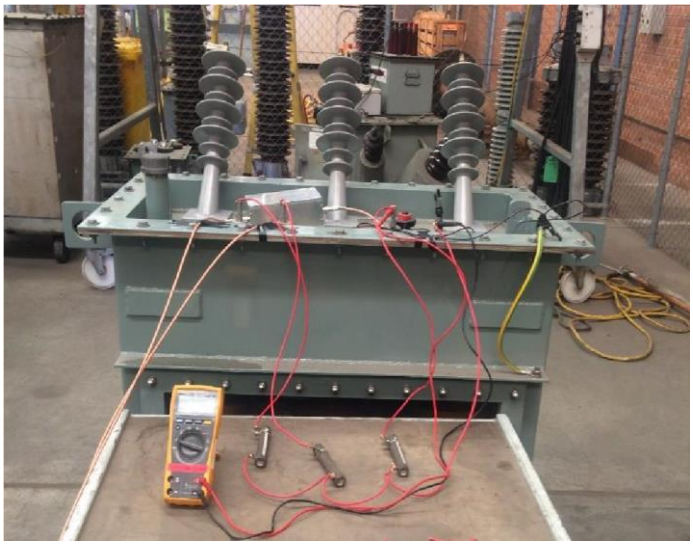

Figure 6.6. Online test setup

the offline IFRA test on phase A of LV winding of the transformer. In this test, the output is the current of grounded neutral point, the input is a 300V nanosecond voltage generated using the Nano-second pulse generator. Transformer offline IFRA signature obtained from the test is depicted in Figure 6.9 (c).

6.3.2 Online Impulse Frequency Response Test

Figures 6.9 (a) and (b) show the input voltage and output current measured from the online IFRA test on phase A of LV winding of the transformer. In this test, 3 phases of transformer HV winding are energized with 11 kV AC. A balanced load of 2 kΩ is connected to all three phases of the transformer LV side.

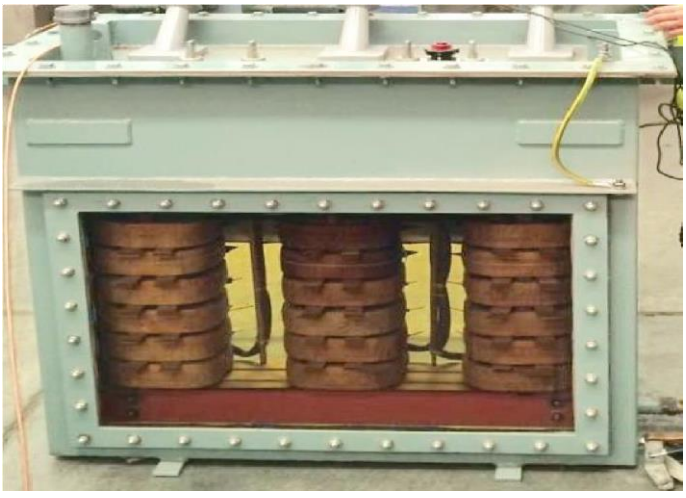

Figure 6.7. Transformer under test

(c)

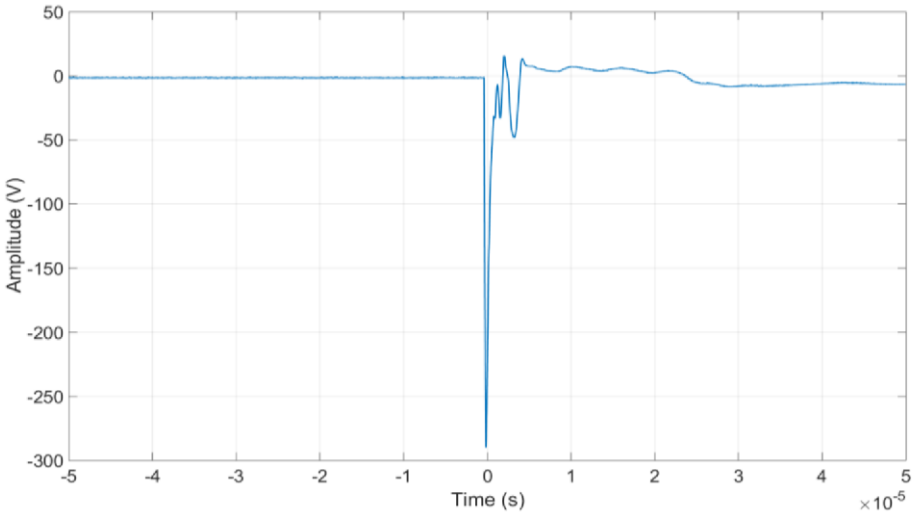

(a)

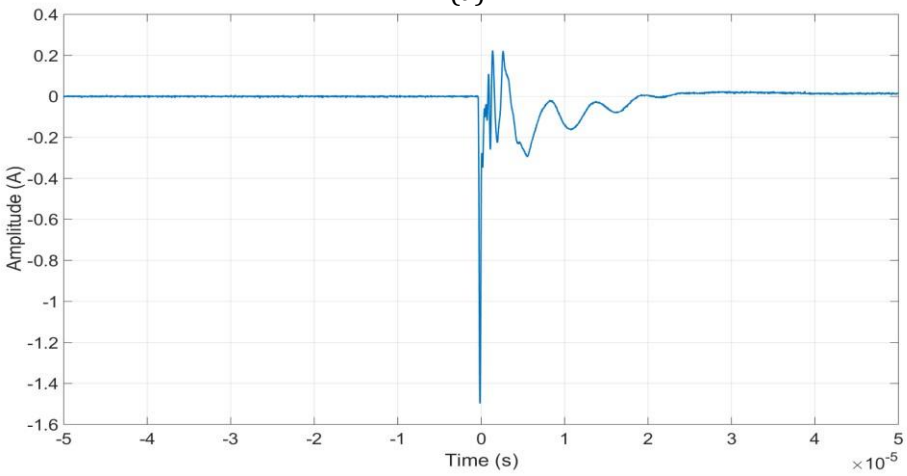

(b)

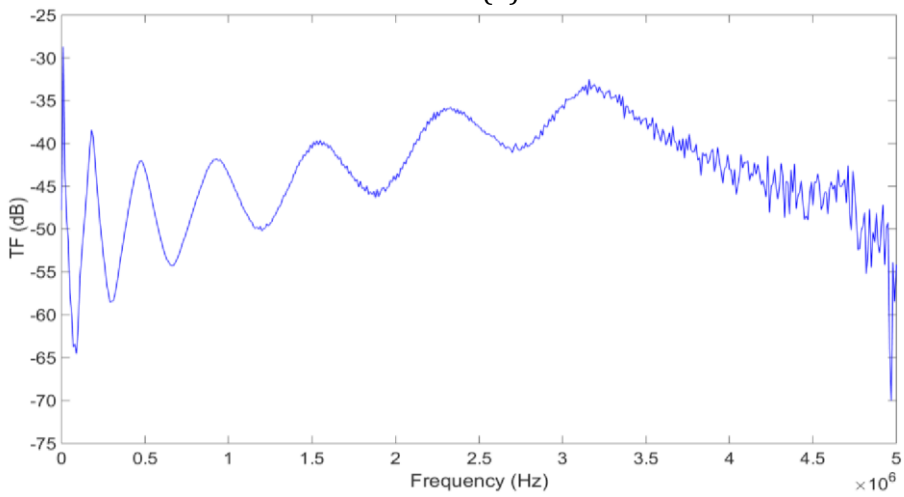

Figure 6.8. Measurement results a) input voltage b)output current c) transformer offline IFRA signature

The output is the current of grounded neutral point, the input is a 1000 V, 300 Nanosecond voltage generated using the Nano-second pulse generator. Transformer online IFRA signature obtained from the test is depicted in Figure 6.9 (c).

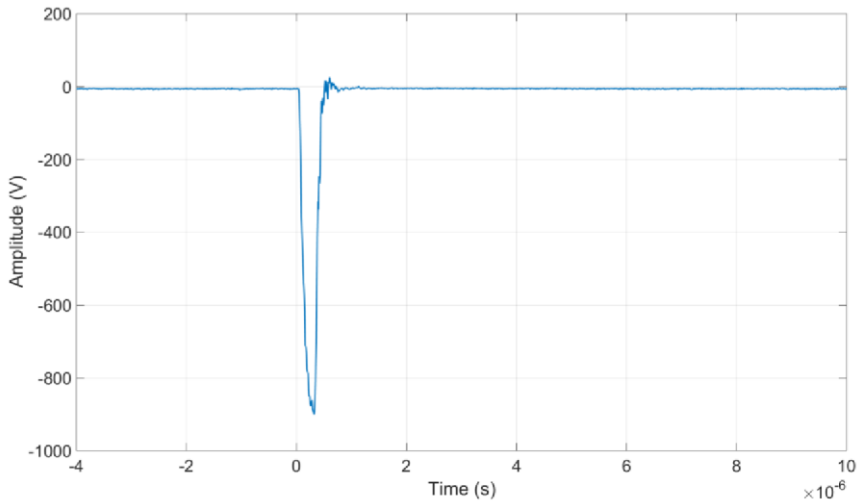

(a)

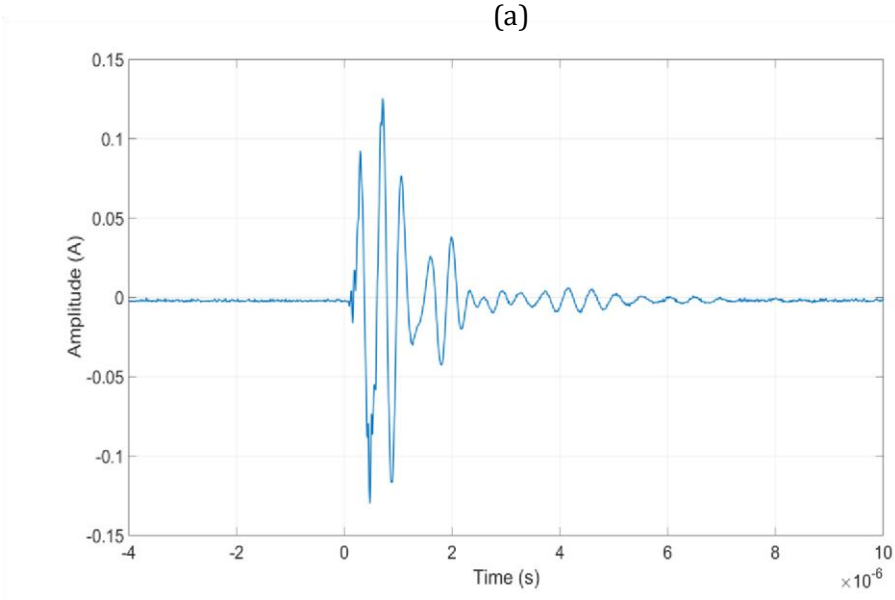

(b)

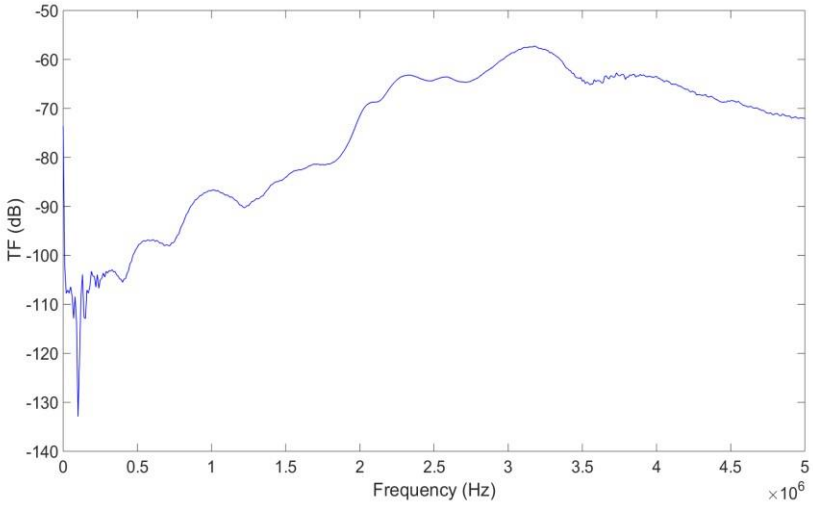

(c)

Figure 6.9. Measurement results a) input voltage b)output current c) transformer offline IFRA signature

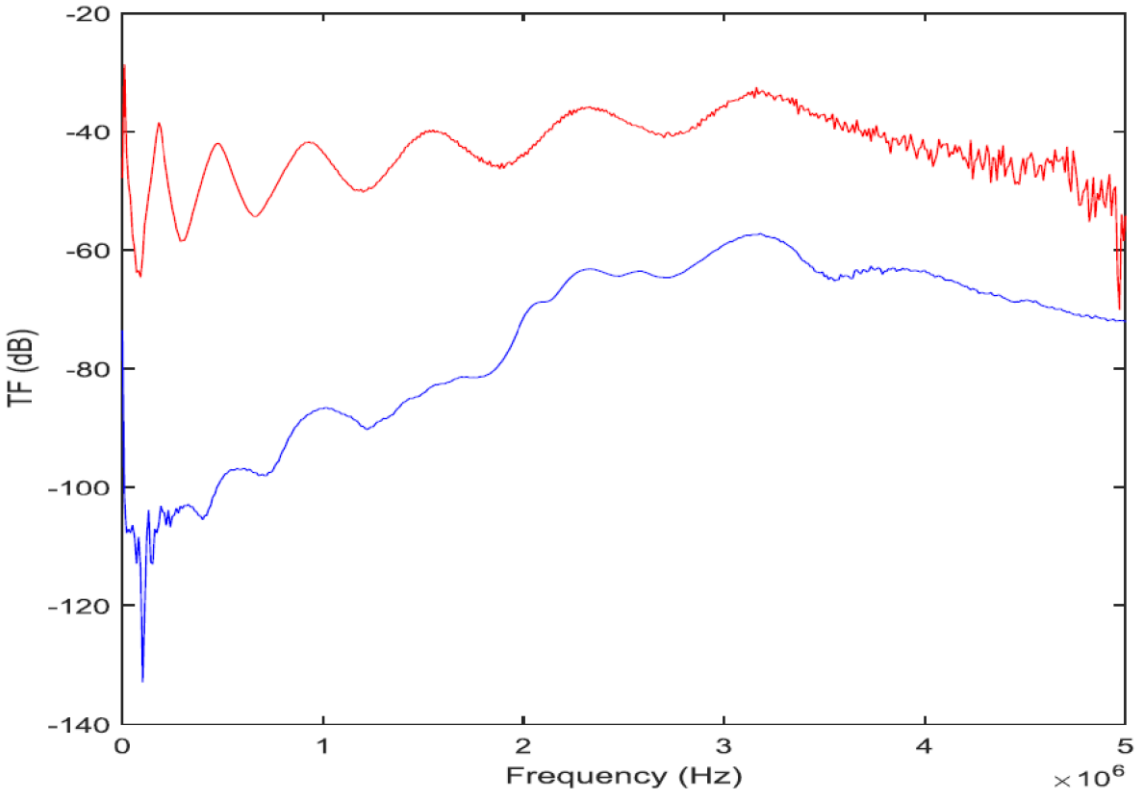

(a)

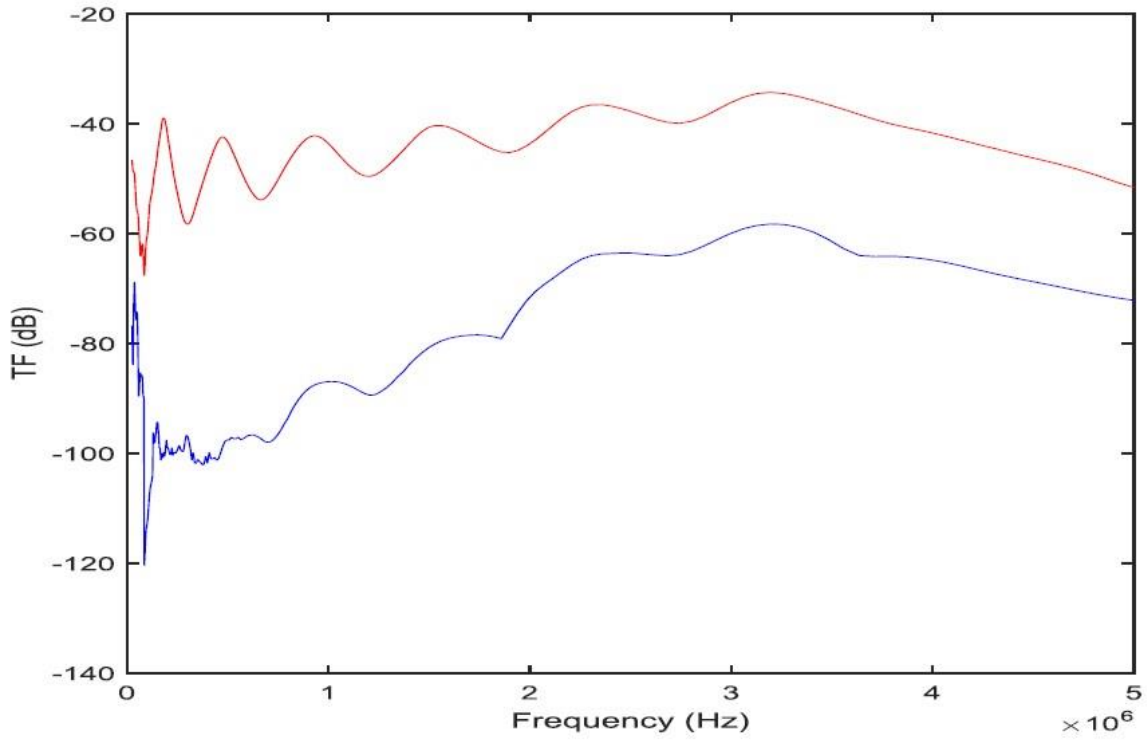

(b)

Figure 6.10. Transformer offline (red) and online (blue) IFRA signatures a) before and b) after applying the filtering technique

6.4 Application of the Proposed Filtering Technique on Test Results

Among the two types of noise under investigation in this study, background noise coming from the measurement device and ambient is present in the test results. As shown in Figure, the presence of background noise adds fault resonance and anti-resonance to the obtained transfer function, masking the inherent resonance and anti-resonance of the transformer which could, in turn, lead to misinterpretation of the results.

The investigation of the impact of pulse-shaped interferences propagating inside the transformer from switching and other phenomena elsewhere in the power grid is yet to be implemented in real time due to limitations of time and facilities. However the filtering technique discussed in previous chapter is applied to the test results to remove the impact of background noise. Figures 6.10(a) and (b) show the IFRA signature of the transformer before and after filtering out the background noise, respectively. As can be seen, after de-noising the signals, the transfer function obtained from the experiment shows a better compatibility with the resonance and anti-resonance seen in the offline test.

7. Conclusion

The key contribution of this thesis is to deal with one of the problems in implementing the transformer frequency response test online. Experimental as well as simulation results from an online IFRA test on a 10 kVA power transformer is presented. Hyperbolic S transform is then used to determine the impact of external interferences on the measured data from online IFRA test. A filtering algorithm is proposed through which the impact of external interferences and noise can be removed from the transformer frequency response. The proposed algorithm can be used as a block before assessment of the transformer winding internal mechanical condition so that the pulse-shaped interferences propagating inside the transformer winding from the power system and background noise coming from the measuring device and ambient does not result in misinterpretation of the results which could, in turn, lead to unnecessary costs for disconnecting the transformer from the power grid because of false alarms.

Further Research

- Additional experimental works to further investigate online IFRA testing method and its effectiveness under varying practical conditions;
- Real-life examination of the IFRA testing of in-service transformers in transmission substations where external inferences and noise are present
- Further tuning and enhancement of on the filter design to move from the customized filter design proposed in this study towards a more general and robust filtering technique for elimination of external interferences from online IFRA signals

References

[1] **C. Bengtsson, "Status and trends in transformer monitoring," *IEEE Transactions on Power Delivery,* vol. 11, pp. 1379-1384, 1996.**

[2] **M. Bagheri, M. S. Naderi, and T. Blackburn, "Advanced transformer winding deformation diagnosis: moving from off-line to on-line," *IEEE Transactions on Dielectrics and Electrical Insulation,* vol. 19, pp. 18601870, 2012.**

[3] **Z. Zhao, C. Yao, X. Zhao, N. Hashemnia, and S. Islam, "Impact of capacitive coupling circuit on online impulse frequency response of a power transformer," *IEEE Transactions on Dielectrics and Electrical Insulation,* vol. 23, pp. 1285-1293, 2016.**

[4] **R. Malewski and B. Poulin, "Impulse testing of power transformers using the transfer function method," *IEEE Transactions on Power Delivery,* vol. 3, pp. 476-489, 1988.**

[5] **S. Birlasekaran and F. Fetherston, "Off/on-line FRA condition monitoring technique for power transformer," *IEEE Power Engineering Review,* vol. 19, pp. 54-56, 1999.**

[6] **R. Malewski, J. Douville, and L. Lavallee, "Measurement of switching transients in 735 kV substations and assessment of their severity for transformer insulation," *IEEE Transactions on Power Delivery,* vol. 3, pp. 1380-1390, 1988.**

[7] **V. Behjat, A. Vahedi, A. Setayeshmehr, H. Borsi, and E. Gockenbach, "Diagnosing Shorted Turns on the Windings of Power Transformers Based Upon Online FRA Using Capacitive and Inductive Couplings," *IEEE Transactions on Power Delivery,* vol. 26, pp. 2123-2133, 2011.**

[8] **M. Wang, "Winding movement and condition monitoring of power transformers in service," University of British Columbia, 2003.**

[9] **R. Wimmer and K. Feser, "Calculation of the transfer function of a power transformer with online measuring data," *Prace Naukowe Instytutu Podstaw Elektrotechniki i Elektrotechnologii Politechniki Wrocławskiej. Konferencje,* vol. 40, pp. 86-90, 2004.**

[10] **T. De Rybel, A. Singh, J. A. Vandermaar, M. Wang, J. R. Marti, and K. Srivastava, "Apparatus for online power transformer winding monitoring using bushing tap injection," *IEEE Transactions on Power Delivery,* vol. 24, pp. 996-1003, 2009.**

[11] **E. Gomez-Luna, G. A. Mayor, and J. P. Guerra, "Application of Wavelet Transform to Obtain the Frequency Response of a Transformer From Transient Signals—Part II: Practical Assessment and Validation," *IEEE Transactions on Power Delivery,* vol. 29, pp. 2231-2238, 2014.**

[12] **C. Yao, Z. Zhao, Y. Chen, X. Zhao, Z. Li, Y. Wang, *et al.*, "Transformer winding deformation diagnostic system using online high frequency signal injection by capacitive coupling," *IEEE Transactions on Dielectrics and Electrical Insulation,* vol. 21, pp. 1486-1492, 2014.**

[13] **T. Leibfried and K. Feser, "Monitoring of power transformers using the transfer function method," *IEEE Transactions on Power Delivery,* vol. 14, pp. 1333-1341, 1999.**

[14] L. T. Coffeen, "System and method for on-line impulse frequency response analysis," ed: Google Patents, 2003.

[15] G. E, x00F, L. mez, G. A. Mayor, J. P. Guerra, D. F. S. Salcedo*, et al.*, "Application of Wavelet Transform to Obtain the Frequency Response of a Transformer From Transient Signals—Part 1: Theoretical Analysis," *IEEE Transactions on Power Delivery,* vol. 28, pp. 1709-1714, 2013.

[17] E. Gomez-Luna, D. Silva, G. Aponte, J. Pleite, and D. Hinestroza, "Obtaining the electrical impedance using wavelet transform from the time response," *IEEE Transactions on Power Delivery,* vol. 28, pp. 12421244, 2013.

[18] Abu-siada A, Hashemnia N, Islam S, Masoum MSA, editors. Impact of transformer model parameters variation on FRA signature. 2012 22nd Australasian Universities Power Engineering Conference (AUPEC); 2012 26-29 Sept. 2012.

[19] Gomez-Luna, E., et al., Current Status and Future Trends in FrequencyResponse Analysis with a Transformer in Service. IEEE Transactions on Power Delivery, 2013. 28(2): p. 1024-1031.

[20] J. A. S. B. Jayasinghe, Z. D. Wang, P. N. Jarman, and A. W. Darwin, "Winding movement in power transformers: a comparison of FRA measurement connection methods," *IEEE Transactions on Dielectrics and Electrical Insulation,* vol. 13, pp. 1342-1349, 2006.

[21] R. P. P. Smeets, L. H. T. Paske, P. P. Leufkens, and T. Fogelberg, "Thirteen Years Test Experience With Short-Circuit Withstand Capability of Large Power Transformers," *Presented at the CIGRE 6th Southern Africa Regional Conference, Cape Town, South Africa,* 2009.

[22] V. Behjat and A. Vahedi, "Analysis of internal winding short circuit faults in power transformers using transient finite element method coupling with external circuit equations," *International Journal of Numerical Modelling,* vol. 26, pp. 425-442, 2013.

[23] E. P. Dick and C. C. Erven, "Transformer Diagnostic Testing by Frequuency Response Analysis," *Power Apparatus and Systems, IEEE Transactions on,* vol. PAS-97, pp. 2144-2153, 1978.

[24] P. Picher, J. Lapworth, T. Noonan, and J. Christian, "MECHANICAL-CONDITION ASSESSMENT OF TRANSFORMER WINDINGS USING FREQUENCY RESPONSE ANALYSIS (FRA)," *Technical Brochure 342,* 2008.

[25] R. Harrington, "Transformer winding buckling deformation fault detection using IFRA – Moving from offline to online," Curtin University, 2016.

[26] A. Kraetge, M. Kruger, H. Viljoen, and A. Dierks, "Aspects of the Practical Application of Sweep Frequency Response Analysis," *Presented at the CIGRE 6th Southern Africa Regional Conference, Somerset West, South Africa,* 2009.

[27] C. A2.26, "Mechanical Condition Assessment of Transformer Windings Using Frequency Response Analysis (FRA)," CIGRE Brochure 342April 2008.

[28] S. V. Kulkarni, *Transformer engineering : design and practice / S.V. Kulkarni, S.A. Khaparde*. New York: New York : Marcel Dekker, Inc., 2004.

[29] G. Bertagnolli, *Short-circuit duty of power transformers*: ABB, 2007.

[30] K. Ludwikowski, K. Siodla, and W. Ziomek, "Investigation of transformer model winding deformation using sweep frequency response analysis," *IEEE Transactions on Dielectrics and Electrical Insulation,* vol. 19, pp. 1957-1961, 2012.

[31] M. Bagheri, M. S. Naderi, and T. Blackburn, "Advanced transformer winding deformation diagnosis: moving from off-line to on-line," *Dielectrics and Electrical Insulation, IEEE Transactions on,* vol. 19, pp. 1860-1870, 2012.

[32] K. G. N. B. Abeywickrama, Y. V. Serdyuk, and S. M. Gubanski, "Exploring Possibilities for Characterization of Power Transformer Insulation by Frequency Response Analysis (FRA)," *IEEE Transactions on Power Delivery,* vol. 21, pp. 1375-1382, 2006.

[33] "Measurement of frequency response," in *IEC 60076-18 Ed.1: Power transformers - Part 18*, ed, 2012.

[34] C. A2.26, "Mechanical Condition Assessment of Transformer Windings Using Frequency Response Analysis (FRA)," CIGRE Brochure 3422008.

[35] A. Shintemirov, W. H. Tang, and Q. H. Wu, "Transformer winding condition assessment using frequency response analysis and evidential reasoning," *IET Electric Power Applications,* vol. 4, p. 198, 2010.

[36] S. Tenbohlen and S. A. Ryder, "Making Frequency Response Analysis Measurements: A Comparison of the Swept Frequency and Low Voltage Impulse Methods," *Proc. of the 13th Int. Symp. on High-Voltage Engineering (ISH2003),* 2003.

[37] A. Ashrafian, M. Naderi, and G. Gharehpetian, "Characterisation of internal incipient faults in transformers during impulse test using index based on S matrix energy and standard deviation," *IET electric power applications,* vol. 6, pp. 225-232, 2012.

[38] L. Satish and A. Saravanakumar, "Identification of Terminal Connection and System Function for Sensitive Frequency Response Measurement on Transformers," *Power Delivery, IEEE Transactions on,* vol. 23, pp. 742-750, 2008.

[39] S. D. Mitchell and J. S. Welsh, "The Influence of Complex Permeability on the Broadband Frequency Response of a Power Transformer," *Power Delivery, IEEE Transactions on,* vol. 25, pp. 803813, 2010.

[40] S. D. Mitchell and J. S. Welsh, "Modeling Power Transformers to Support the Interpretation of Frequency-Response Analysis," *Power Delivery, IEEE Transactions on,* vol. 26, pp. 2705-2717, 2011.

[41] A. Kraetge, M. Kruger, and P. Fong, "Frequency Response Analysis - Status of the worldwide standardization activities," ed, 2008, pp. 651-654.

[42] Stockwell, R.G., L. Mansinha, and R.P. Lowe, Localization of the complex spectrum: the S transform. IEEE Transactions on Signal Processing, 1996. 44(4): p. 998-1001.

[43] G. Lian, Y. Ruoping, and C. Pizhang, "An Equivalent Magnetization Surface Current Approach of Calculation 3-Dimensional Leakage Fields of

a Transformer," *Power Delivery, IEEE Transactions on,* vol. 2, pp. 817-822, 1987.

[44] D. A. K. Pham, T. M. T. Pham, H. Borsi, and E. Gockenbach, "A new diagnostic method to support standard frequency response analysis assessments for diagnostics of transformer winding mechanical failures," *Electrical Insulation Magazine, IEEE,* vol. 30, pp. 34-41, 2014.

[45] Z. W. Zhang, W. H. Tang, T. Y. Ji, and Q. H. Wu, "Finite-Element Modeling for Analysis of Radial Deformations Within Transformer Windings," *Power Delivery, IEEE Transactions on,* vol. 29, pp. 22972305, 2014.

[46] E. Rahimpour, J. Christian, K. Feser, and H. Mohseni, "Transfer function method to diagnose axial displacement and radial deformation of transformer windings," *Power Delivery, IEEE Transactions on,* vol. 18, pp. 493-505, 2003.

[47] E. Rahimpour, M. Vakilian, and M. Bigdeli, "A New Method for Detection and Evaluation of Winding Mechanical Faults in Transformer through Transfer Function Measurements," *Advances in Electrical and Computer Engineering,* vol. 11, pp. 23-30, 2011.

[48] P. Karimifard, G. B. Gharehpetian, and S. Tenbohlen, "Localization of winding radial deformation and determination of deformation extent using vector fitting-based estimated transfer function," *European Transactions on Electrical Power,* vol. 19, pp. 749-762, 2009.

[49] A. Setayeshmehr, A. Akbari, H. Borsi, and E. Gockenbach, "On-line monitoring and diagnoses of power transformer bushings," *Dielectrics and Electrical Insulation, IEEE Transactions on,* vol. 13, pp. 608-615, 2006.

[50] V. Behjat, A. Vahedi, A. Setayeshmehr, H. Borsi, and E. Gockenbach, "Diagnosing Shorted Turns on the Windings of Power Transformers Based Upon Online FRA Using Capacitive and Inductive Couplings," *Power Delivery, IEEE Transactions on,* vol. 26, pp. 2123-2133, 2011.

[51] M. Guo-Ming, L. Cheng-Rong, Q. Jiang-Tao, and J. Jian, "Measurement of VFTO Based on the Transformer Bushing Sensor," *Power Delivery, IEEE Transactions on,* vol. 26, pp. 684-692, 2011.

[52] Z. Zhao, C. Yao, X. Zhao, N. Hashemnia, and S. Islam, "Impact of capacitive coupling circuit on online impulse frequency response of a power transformer," *IEEE Transactions on Dielectrics and Electrical Insulation,* vol. 23, pp. 1285-1293, 2016 2016.

[53] Amini A, Das N, Islam S, editors. Impact of buckling deformation on the FRA signature of power transformer. 2013 Australasian Universities Power Engineering Conference (AUPEC); 2013 Sept. 29 2013-Oct. 3 2013.

[54] S. M. Islam, "Detection of shorted turns and winding movements in large power transformers using frequency response analysis2000 IEEE Power Engineering Society Winter Meeting Conference Proceedings; 2000 23-27 Jan 2000.